HHS Public Access

Author manuscript

Eur J Nanomed. Author manuscript; available in PMC 2017 July 01.

Published in final edited form as:

Eur J Nanomed. 2016 July ; 8(3): 151–170. doi:10.1515/ejnm-2016-0011.

Radio-nanomaterials for biomedical applications: state of the art

Weifei Lu,

Department of Radiology, University of Michigan – Ann Arbor, MI 48109-2200, USA; and College of Animal Sciences and Veterinary Medicine, Henan Agriculture University, Zhengzhou, Henan 450002, China

Hao Hong, and

Department of Radiology, University of Michigan – Ann Arbor, MI 48109-2200, USA, Phone: +1-734-615-4634, Fax: +1-734-615-1599, hahong@med.umich.edu;

Weibo Cai

Department of Radiology and Medical Physics, University of Wisconsin – Madison, WI 53705-2275, USA; and University of Wisconsin Carbone Cancer Center, Madison, WI 53705-2275, USA, Phone: +1-608-262-1749, Fax: +1-608-265-0614, wcai@uwhealth.org

Abstract

The incorporation of radioactive isotope(s) into conventional nanomaterials can bring extra properties which are not possessed by original materials. The resulting radioactive nanomaterials (radio-nanomaterials), with added physical/chemical properties, can be used as important tools for different biomedical applications. In this review, our goal is to provide an up-to-date overview on these applications using radio-nanomaterials. The first section illustrates the utilization of radionanomaterials for understanding of in vivo kinetics of their parent nano-materials. In the second section, we focus on two primary applications of radio-nanomaterials: imaging and therapeutic delivery. With various methods being used to form radio-nanomaterials, they can be used for positron emission tomography (PET), single-photon emission computed tomography (SPECT), and multimodal imaging. Therapeutic isotopes-loading radio-nanomaterials can possess selective killing efficacy of diseased cells (e.g. tumor cells) and can provide promises for certain isotopes which are not able to be used in a conventional manner. The successful and versatile biomedical applications of radio-nanomaterials warrants further investigations of those materials and their optimizations can pave the way to future imaging guidable, personalized treatments in patients.

Graphical abstract

Review: With proper functionalization and cargo loading, radioactive nano-materials can prove to be extremely useful tools for material pharmacokinetic determination, imaging (diagnosis) of diseases, and therapeutic delivery into the diseased sites.

Correspondence to: Hao Hong; Weibo Cai.

Conflict of interest statement: The authors state no conflict of interest. All authors have read the journal's publication ethics and publication malpractice statement available at the journal's website and hereby confirm that they comply with all its parts applicable to the present scientific work.

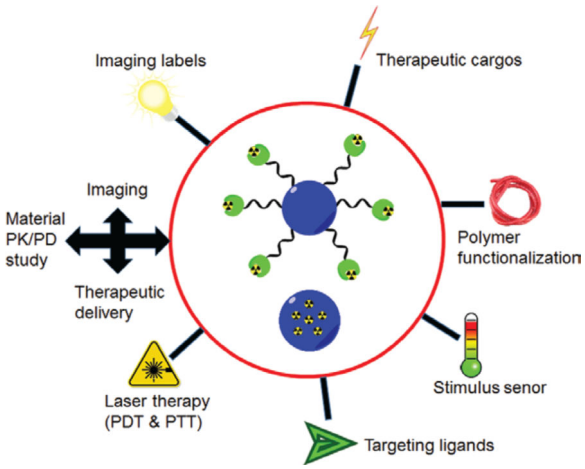

Keywords

in vivo distribution; positron emission tomography; radiation therapy; radioactive nanomaterials; radiolabel; single-photon emission computed tomography

Introduction

In the past several decades, numerous nanoscale materials (size range: several to a few 100 nm) have been developed for a wide range of biomedical applications including but not limited to drug delivery, sensing, disease detection, and tissue engineering (1). With unique physical/chemical properties, these materials provided unparalleled opportunities to improve diagnostic accuracy and add treatment alternatives available to patients, especially those with different types of cancer (2–4). Several drug nanoformulations have been approved clinically (e.g. Doxil) which possess optimized pharmacokinetic profiles when compared with the original drug: reduced side effects, improved therapeutic index, etc. (5). Despite the proven success, great efforts have been continuously invested in the development of novel nanomaterials with more potent disease targeting or therapeutic capability, optimized in vivo kinetics, and enhanced cargo-loading efficiency.

Compared with conventional nanomaterials, radioactive nanomaterials (radio-nanomaterials, Scheme 1) have more appealing characteristics due to the synergistic integration of unique physical/chemical properties from radionuclides into nanomaterials (6). On the one hand, the incorporation of radioisotope(s) bestows extra tracking/therapeutic ability to the nanomaterial where radioisotope(s) on nanomaterial acts as an energy donor. Most radio-nanomaterials are useful contrast agents for positron emission tomography (PET) or single-photon emission computed tomography (SPECT) imaging. On the other hand, suitable nanomaterials may serve as carriers to accommodate certain “unconventional” isotopes so that they can be used in biomedical applications otherwise very difficult to achieve. A few examples include radioactive arsenic (e.g. ^{72}As) (7, 8), gemanium-69 (^{69}Ge) (9), or sodium-22 (^{22}Na) (10). With careful design and optimization, radio-nanomaterials can be utilized as effective theranostic agents.

Three elements have to be taken into consideration before the production of a radio-nanomaterial, which include the choice of a suitable isotope (or isotopes), the selection of a nanomaterial with desired properties, and a method to integrate the isotope effectively into the nanomaterial (11). For a given biomedical application, the isotope can be used as either an imaging label (e.g. for PET or SPECT), or a therapeutic moiety, or both (6). The integrity of radio-nanomaterial is extremely important for their biomedical applications, and herein this integrity refers to two aspects: the isotope should not be released prematurely from the nanomaterial, and the nanomaterial itself should possess sufficient stability. In addition, radio-nanomaterials should not pose significant acute or chronic toxicity to the test subject. The intrinsic properties from nanomaterial can sometimes boost the performance of the loaded isotope in vivo, e.g. stimuli-responsive release of the isotope, or energy transfer for imaging applications (12).

An optimal method for isotope incorporation should be fast, efficient, and should impose minimal changes to the characteristics of the chosen nanomaterial. For detailed information on how an isotope can be incorporated into the nanomaterial (the radiolabeling/radiochemistry methods), or distinct nuclear reactions to obtain appropriate isotopes for these applications, interested readers can resort to references (6, 11). In brief, four strategies are currently used for radio-nanomaterial production: 1) synthesis of a radio-nanomaterial with an isotope precursor; 2) post-synthesis chemical linking (e.g. using a chelating agent for radiometals) or physical absorption; 3) post-synthesis isotope exchange; 4) material activation/bombardment by neutron/proton beams. The choice of strategies may affect the amount of the isotope loadable on the material, and impact the stability of resulting nanomaterials.

In this review, we will try to summarize the recent progress in radio-nanomaterials for biomedical applications. The utilization of radio-nanomaterials for clarifying in vivo material distribution/pharmacokinetics will be introduced in the first place. In the following sections, the biomedical applications of radio-nanomaterials will be categorized into two primary aspects: imaging and therapeutic applications. In the last section, future perspectives of new biomedical applications of radio-nanomaterials are given. Although the research on radio-nanomaterials literally started <10 years ago, a large number of radio-nanomaterials have been produced.

In vivo kinetics of radio-nanomaterials

Fabrication of radio-nanomaterials can help to noninvasively monitor the pharmacokinetics of parent materials inside a living subject and collect relevant knowledge on their organ absorption, distribution, metabolism (clearance), stability, and drug release kinetics, etc. This information can be critical to judge whether these nanomaterials are suitable for a given application, e.g. therapeutic delivery to a given diseased site.

Metabolic study of nanomaterials

The first example to illustrate the usefulness of radio-nanomaterial for metabolic study is the rodent safety evaluation of zerovalent iron nanoparticles (nZVI) (13), which are used for ground water decontamination. Whole-body retention and metabolic activity of neutron-

activated radioactive ^{59}Fe-nZVI was assessed in mice post oral gavage. The findings indicated that the majority of ^{59}Fe-nZVI was rapidly excreted via the feces in 24 h with a small amount of radioactivity retained in the liver after three repeated daily doses. This information is extremely helpful to adjust the nZVI dose during the water processing for human consumption. Proton activated, nitrogen-13 (^{13}N) labeled aluminum oxide nanoparticles [^{13}N-Al_2O_3 NPs, via the ^{16}O(p, α) ^{13}N reaction] were used within another study to determine the material distribution pattern in rats, monitored by PET (14). The appearance of ^{13}N into Al_2O_3 NPs did not alter their surface or structural properties. Al_2O_3 NPs demonstrated a biexponential decay in vivo and the relationship between particle size and organ distribution pattern could be determined after intravenous administration (Figure 1A).

In certain situation, different radiolabels can be tethered on the same nanomaterial to provide complementary and more accurate information on its distribution profile. For instance, oleic acid functionalized iron-oxide nanoparticles (IONPs) were separately radiolabeled with ^{59}Fe, ^{14}C-oleic acid, and ^{111}In for studying their organ distribution in mice (16). Although all the radioactive signals preferentially localized in liver, spleen and bone, stronger signal levels from ^{59}Fe were observed in liver and spleen than those from ^{111}In, but lower than those from ^{14}C. This technique can be of great value to clarify the kinetics of different components from the same nanomaterial.

Radio-nanomaterials were also useful for evaluation of cargo integrity or material stability. For instance, dasatinib, an inhibitor for platelet-derived growth factor receptor, was loaded into a micellar liposome nanoformulation for enhanced tumor retention. Instead of providing radiolabels on micelles, ^{18}F was introduced into the molecular structure of dasatinib to produce ^{18}F-SKI249380. The stability and distribution of dasatinib micelles was estimated in a genetically engineered mouse model of high-grade glioma (17). Better tumor accumulation and retention was observed for ^{18}F-SKI249380-containing micelle formulations compared to free ^{18}F-SKI249380, and ^{18}F-SKI249380-containing micelle formulations possessed good stability judging from their kinetic behaviors. As intra-tumor drug concentrations can be calculated from this study, this method can facilitate treatment planning with dasatinib. In another study, the stability of titanium implants was evaluated in rats by coating with hydroxyapatite (HA) nanoparticles and labeled with calcium-45 (^{45}Ca) (18). At different time points post-implantation, the implants and surrounding bone were retrieved and analyzed by autoradiography to determine particle migration from the implant surface. Major tissues and metabolic excretions were also retrieved and analyzed by liquid scintillation counting. The radioactivity of ^{45}Ca decreased over time from the vicinity of the implant into the blood and eventually appeared in the animal excretions. After 8 weeks, only trace amount of ^{45}Ca could be found in the liver. The results confirmed the safety of the nano-coating instead of being considered a potential biologic risk factor.

With proper radiolabels, in vivo tracking of nanomaterials can prepare them for new applications. For example, a rare-earth cation exchange method was used to introduce samarium-153 (^{153}Sm) into lanthanide based upconversion nanoparticles (UCNPs) and enabled the tracking of their in vivo behaviors (19). By SPECT imaging, it was demonstrated that UCNPs were mainly captured by the mononuclear phagocyte system

(MPS, primarily liver and spleen), and the accumulation of UCNP in liver was faster and was about 15-fold of that in spleen. This information about distribution/excretion of UCNPs in vivo can be extremely helpful before they can be used as a contrast agent for detection of a specific disease. Similar technique was used by the same group to monitor in vivo behavior of UCNPs with different chemical compositions and different synthesis method (20). In another study, ^{99m}Tc-labeled mannosylated Gantrez nanoparticles were studied in mice for their organ distribution (post-loading with the *Brucella ovis* antigen) after ocular administration (21). The accumulation of these nanoparticles in nasal and ocular mucosa and gastrointestinal tract was observed, confirming its value as an effective antigenic delivery system through the ocular mucosa. These nanoparticles can trigger elevated immune response and provide protection against *Brucella* to serve as a vaccine candidate. A more recent case is to evaluate distribution and clearance profile of indium-111 (^{111}In) labeled albumin-based nanomaterials and prepare them for pulmonary drug delivery (22). ^{111}In labeled albumin nanoparticles [via coordination with diethylenetriaminepentaacetic acid (DTPA)] demonstrated a slow clearance from the mouse lung with significant retention the lung tissue rather than the lung fluid. Low amounts of ^{111}In activity were also detectable in the liver, kidneys, and intestine post 24 h, indicating clearance by translocation across the lung mucosal barrier. This study provides important information on the fate of albumin vehicles in the lungs, which may direct future design of inhaled nanomedicines.

Factors to affect nanomaterial distribution

The distribution profile of a given nanomaterial can be affected by different factors (e.g. administration routes, size, morphology, etc.), and radio-nanomaterials can help to determine the importance of each factor. For example, both fluorine-18 (^{18}F) (23) and zinc-65 (^{65}Zn) (24) were used to study in vivo distribution of zinc oxide (ZnO) nanoparticles via different administration routes. In those studies, ^{18}F-labeled ZnO nanoparticles (via click chemistry) showed observable radioactivity in the lung, liver, kidney, and the GI tract after oral administration (23). Increased size of ZnO nanoparticles (e.g. from 20 nm to 100 nm) resulted in higher accumulation in the liver and kidney. Compared with ^{18}F-labeled ZnO nanoparticles, intravenous injection of ^{65}ZnO nanoparticles resulted in preferential accumulation in the liver and spleen at 24 h while radioactivity of ^{65}Zn was also detectable in bone, brain, lung, heart and kidneys after 4 weeks (80% excretion was observed at that time) (24). Although the size of the ZnO nanoparticles did not play a significant role in determination of in vivo kinetics, smallersized ZnO nanoparticles had longer retention time in some organs.

The impact of administration routes on material distribution profile can also be clarified, capitalizing on the localization of radio-nanomaterials. In an early study, the pharmacokinetic behaviors of ^{111}In-labeled, PEGylated liposomes were evaluated in a peritoneal tumor model in mice (25). In this particular tumor model, intraperitoneal (i.p.) injection could result in more effective retention of liposomes compared with intravenous (i.v.) injection, thus being considered as better treatment approach. More recently, copper-64 (^{64}Cu) was used as a radiolabel for gold nanoshells [via 1,4,7,10-tetraazacyclododecane-1,4,7,10-tetraacetic acid (DOTA) chelation] in order to provide a systematic investigation on their distribution pattern in tumor-bearing rats via different

injection routes (26), as some studies indicated that passive delivery of gold nanoshells through intravenous administration resulted in limited tumor accumulation. From the acquired pharmacokinetic curves, intratumor administration showed higher retention of ^{64}Cu-nanoshells in tumors and less concentration in other healthy organs. ^{64}Cu-labeled hollow gold nanospheres (HAuNS) were evaluated in a rabbit liver tumor model to compare tumor uptakes from different injection routes (27). Animals with hepatic intra-artery injection of arginine-glycine-aspartate (RGD) peptide-conjugated HAuNS showed significantly higher tumor uptake and higher tumor-to-normal liver ratios in all other groups.

The relationship between surface charges/material morphology and material pharmacokinetic behavior can also be studied with radio-nanomaterials. In one study, the tissue distribution of nanostructured lipid carriers (NLCs, radiolabeled with ^{99m}Tc) with different surface charges and sizes was evaluated after their intravenous administration to rats (28). No differences on the mean residence time in blood among the NLCs were observed in spite of these differences. Higher accumulation in the kidney was observed for those NLCs with positive charges, while NLCs with negative charge accumulated preferably in the liver. NLCs with larger particle size showed a higher uptake in the lung and lower accumulation in liver and bone marrow, in comparison with the smaller ones. Another interesting study explored the impact of material shapes on their distribution pattern in vivo (15). Different Au nanostructures (i.e. nanospheres, nanodisks, nanorods, and cubic nanocages) with a similar size were synthesized with the incorporation of ^{198}Au into the crystal lattice for organ distribution evaluation in a murine EMT6 breast cancer model. Significantly higher tumor uptake was observed for the Au nanospheres and nanodisks relative to the Au nanorods and nanocages within the observing time frames (monitored by Cerenkov luminescence, Figure 1B). Furthermore, intratumoral distributions from autoradiography confirmed that nanospheres and nanodisks were only observed on the surfaces of the tumors, while nanorods and nanocages had a more even distribution throughout the tumors. Proper determination of nanomaterial pharmacokinetics from the usage of radio-nanomaterials will provide invaluable insights to guide the design of more effective imaging/therapy vectors discussed in the below sections.

Imaging

Many radio-nanomaterials are natural imaging contrast agents for PET and SPECT imaging due to the existence of radioisotopes. Image conspicuity can be enhanced from their utilization for lesion detection. Nanomaterials can be of great valuable for diagnostic applications since they can serve as selective carriers of a radioisotope to a particular region of interest (ROI) with good accuracy. In addition, the benefits of nanomaterials as imaging agents include large surface area to volume, versatile surface chemistry to integrate multiple targeting ligands, and excellent cargo-carrying capacity for multimodal imaging.

PET or SPECT

Nuclear imaging modalities (PET and SPECT) provide highly sensitive detection of biological events in vivo, particularly useful for disease diagnosis, staging, and treatment response evaluation (29). Conventional isotopes for PET or SPECT imaging can be

seamlessly integrated into nanomaterials and create new applications for them, for example, zirconium-89 (^{89}Zr) (30), ^{64}Cu (31), or ^{111}In (32). Most of these radio-nanomaterials were confirmed to be sufficiently stable in vivo with acceptable biocompatibility.

Cancer imaging

Radio-nanomaterials are particularly suitable for imaging of cancer as most nanomaterials with diameters in the range of 5–200 nm have good enhanced permeability and retention (EPR) effect to tumor sites, which means that they can have a significant accumulation in tumor even without a targeting ligand (33). Different radiolabeled, inorganic [e.g. silica- or carbon-based, gold nanomaterials, quantum dots (QDs), etc.] or organic (polymer-based, liposomal nanomaterials, etc.) nanomaterials have been used for detection of primary/metastatic tumors and imaging guided therapeutic delivery (34, 35). The majority of nanomaterials have some unique physical properties which can be applicable for different imaging techniques (e.g. gold nanomaterials can be used for fluorescence or photo-acoustic imaging, QDs can be used for fluorescence imaging, or IONPs can be used for MRI). In addition, some nanomaterials can have inherent physicochemical properties to enable them to accumulate in certain types of cancer. For example, ^{99m}Tc-labeled HA nanoparticles can be used for imaging of bone tumors (36). However, to enhance the capture of nanomaterials by cancerous tissues, most radio-nanomaterials need to be attached to “targeting” ligands (which usually possess strong affinity against an up-regulated biomarker during cancer progression) (37).

Good examples include graphene-based nanosheets labeled with ^{66}Ga (38), ^{64}Cu (39, 40), or ^{111}In (41) for PET (SPECT) imaging of breast cancer. With the attachment of different targeting ligands (e.g. antibodies, proteins, etc.), the tumor accumulation of those nano-graphene was sufficient to prepare them for future targeted photothermal therapy of tumors. Silicabased nanomaterials are another attractive contrast agents for PET (SPECT) imaging of cancer. For example, mesoporous silica nanoparticle (MSN) or hollow MSN (hMSN, Figure 2A) was labeled with ^{64}Cu and an antibody against an angiogenesis target CD105 for PET-guided, enhanced drug delivery to 4T1 murine breast cancer model (42, 44). A good overview on imaging applications with mesoporous silica nanomaterials can be found elsewhere (45).

Gold nanomaterials are a standout category of inorganic nanomaterials which are frequently used for cancer imaging. For example, water-soluble, maleimideterminated PEGylated gold nanoparticles (AuNPs) were radiolabeled by the [^{18}F]-silicon-fluorine prosthetic group and attached by a cysteine-modified octreotate (binds to somatostatin receptor [SSTR] subtypes 2 and 5) for delineation of brain tumors (46). Aptamer- and antibody (C225)-coated HAuNS (both targeted to epidermal growth factor receptors [EGFR]) were evaluated in another report for targeting of human OSC-19 oral tumors (EGFR^{+}) post labeling with ^{111}In (47). Both antibody-conjugated and aptamer-conjugated HAuNS demonstrated good tumor uptake, and SPECT/CT confirmed that there was even higher tumor uptake from aptamer-conjugated HAuNS. Using a chelator-free radiolabeling method, ^{64}Cu was chemically reduced onto the surface of PEG-stabilized Au nanorods (48). These ^{64}Cu-incorporated, RGD-conjugated Au nanorods showed potent tumor targeting ability in a U87MG

glioblastoma xenograft model and were successfully used for image-guided photothermal tumor therapy.

Radioactive organic nanomaterials are also beneficial contrast agents for cancer detection. Among them, nanosized liposomes were frequently adopted for tumor imaging (49, 50). For example, PEG-coated liposome was modified with a monoclonal antibody 2C5 (against nucleosome overexpressed in tumors) for SPECT imaging of tumor (^{99m}Tc was encapsulated as a radiolabel) (51). ^{99m}Tc-2C5-PEG-liposomes demonstrated potent uptake in different tumor types, and the tumor uptake was 3–8 fold higher than non-targeted liposomes. Another study adopted a dual targeting strategy for ^{111}In-labeled liposomal nanoparticles via integrin (by RGD) and neurokinin-1 (by substance P peptide) overexpressed in glioma and melanoma (52). However, SPECT studies in tumor- bearing mice unexpectedly revealed only moderate tumor uptake and no observable synergistic effect using this dual-targeting approach. SSTR-targeted polyamidoamine (PAMAM) dendrimers were used recently for targeting of neuroendocrine tumors (53). ^{99m}Tc-PAMAM-Tyr3-octreotide showed specific accumulation in AR42J tumors and the pancreas (both SSTR^{+}), with a significant renal excretion.

Aside from traditional “tumor detection”, radio-nanomaterials are also useful for imaging of tumor associated markers/cell populations. One good example is tumorassociated macrophages (TAMs), which are considered to have high diagnostic and prognostic value for various cancer types (54). Imaging of TAM is considered as largely unexplored, before a recent study described the development of ^{89}Zr-labeled, reconstituted high-density lipoprotein (HDL)-nanoparticles for PET imaging of TAM in a murine model of breast cancer (43). Intravenous administration of ^{89}Zr-labeled HDL nanoparticles (with two formulations) resulted in potent tumor accumulation at 24 h after injection (Figure 2B). Histologic analysis showed good localization of radioactivity with TAM-rich areas in tumor sections. Thus, these ^{89}Zr-rHDL imaging agents could be valuable for noninvasive monitoring of TAM and assessing relevant therapeutic interventions. Other important applications for radio-nanomaterials include noninvasive lymph node (LN) mapping – especially for tumor-drained LNs. Their advantages and limitations have been thoroughly summarized in a recent review article (55).

Imaging of other diseases

Radio-nanomaterials have also been used for imaging/ diagnosis of other diseases, for example, inflammation, or cardiovascular diseases. In one study, ^{89}Zr-labeled dextran nanoparticle (DNP) was used for imaging of monocytes and macrophages, as biomarkers of atherosclerotic plaques progression (56). PET imaging revealed higher uptake of ^{89}Zr-DNP in the aortic root of apolipoprotein E knock out (ApoE$^{-/-}$) mice than that of wild-type controls (corroborated by autoradiography) while silencing of monocytes decreased ^{89}Zr-DNP accumulation in the plaque. ^{89}Zr-DNP enabled noninvasive assessment of inflammation in atherosclerotic plaques and could provide feedback on therapeutic efficacy of anti-inflammatory therapy. Poly (methyl methacrylate)-core/ polyethylene glycol-shell amphiphilic comblike nanoparticles were used in another study for detection of atherosclerotic lesions in ApoE$^{-/-}$ wire-injury mice (57). These nanoparticles were labeled

with ^{64}Cu and conjugated with D-Ala1-peptide T-amide (DAPTA) peptide (a selective ligand for chemokine receptor 5 [CCR5]), and they showed better accumulations in the injury lesions compared with those at the sham-operated sites (Figure 3A). This nanoplatform can provide sensitive and specific detection of CCR5 for clarification of its biological functions in atherosclerosis. In addition, ^{99m}Tc-labeled, methoxypolyethylene glycol-graft-poly (L-lysine) copolymer (mPEG-gPLL) stabilized AuNPs was also produced recently for detection of induced inflammation (Figure 3B) (58).

Chitosan hydrogel nanoparticles loaded with VEGF fragments (labeled with ^{99m}Tc) are considered as a good example for targeting of ischemic myocardium (59). Rats with myocardial ischemia were injected with chitosan hydrogel nanoparticles labeled with $VEGF_{165}$ or $VEGF_{81–91}$ peptides via apical puncture. Ischemic hearts receiving chitosan without tethering VEGF fragments served as the control group. SPECT imaging revealed that both chitosan-$VEGF_{165}$ and chitosan $VEGF_{81–91}$ possessed more potent absorption in the ischemic sites and reduced the degree of perfusion defects.

Imaging of other biological process

Radio-nanomaterials can also be used for studying some complex biological process. For example, ^{153}Sm-labeled UCNPs coated with polyphosphoric acid ligand were used for SPECT imaging of blood pool (60). These radiolabeled UCNPs demonstrated superior circulation time in mice, which is possibly due to the adhesion of these UCNPs on the membrane of red blood cells. Another interesting study used ^{68}Ga-labeled, glucose-coated AuNPs [which carried blood-brain barrier (BBB)-permeable peptides] to visualize the drug permeability across the BBB (61). Organ distribution of AuNPs was evaluated in rats by PET after intravenous administration. One peptide candidate-conjugated ^{68}Ga-AuNPs managed to show beneficial BBB crossing (near 3-fold higher) compared to non-targeted AuNPs.

Cerenkov imaging

Radioactive nanomaterials can prove to be a cost-effective alternative for laboratories equipped with optical imaging instruments by using the Cerenkov imaging technique. This imaging method is based on the electromagnetic radiation produced when a charged particle (e.g. positron, electron, etc.) travels faster than the light speed in an insulating medium (62). When radioisotopes are incorporated onto nanomaterials with optical properties (e.g. QDs or AuNPs), Cerenkov luminescence emitted from radioisotopes can serve as an excitation source (an energy donor) to trigger fluorescence from these nanomaterials, and it is named Cerenkov radiation energy transfer (CRET).

Based on this concept of CRET, self-illuminating QDs (structure: CuInS/ZnS) were developed in one study by using $^{64}CuCl_2$ as a synthesis precursor (63). With excellent radiochemical stability, PEGylated ^{64}Cu-QDs showed high tumor uptake in U87MG mouse xenografts and were successfully applied as an efficient PET/CRET agent for in vivo usage. Self-illuminating QDs can also be constructed by doping ^{64}Cu into CdSe/ZnS core/shell QDs via a cationexchange reaction (64). The resulting ^{64}Cu-doped CdSe/ ZnS QDs also exhibited strong CRET properties and good tumor-targeting ability in U87MG xenografts.

Another interesting study used different lengths of DNA as a linker between ^{64}Cu and QDs (65). Cerenkov radiation from ^{64}Cu was able to excite the QDs in a distance-dependent manner to make this radiolabeled QD a so-called “nano-ruler”.

Radiolabeled gold nanomaterials are attractive as CRET contrast agents due to their better biocompatibility (than QDs) and optimal fluorescence excitation/emission. ^{198}Au was used recently to form radioluminescent Au nanocages via a precursor-based method (66). Under biological conditions these ^{198}Au nanocages can emit light in the wavelengths of visible and near-infrared regions, enabling luminescence imaging of the whole mice in vivo. With a similar design, ^{64}Cudoped gold nanoclusters (AuNCs) were developed for PET/CRET dual modal imaging (67), in which AuNCs acted as the energy acceptor to produce NIR fluorescence. In U87MG xenografts, ^{64}Cu-doped AuNCs produced prominent tumor accumulation, confirmed from self-illuminating NIR images in the absence of external excitation.

Multimodality imaging

Different imaging labels can be integrated into one nanomaterial to be detectable by different imaging techniques simultaneously. Each imaging modality has its own pros and cons (68), for example PET and SPECT have excellent detection sensitivity (down to 10^{-12} M)/depth and quantitative capacity, while they possess relatively low image spatial resolution. MRI gives fine anatomical information however its detection sensitivity is not optimal. Optical imaging is safe and cost-effective, and can provide surgical guidance, however the narrow tissue penetration depth (usually <1 cm) is the primary limiting factor for detection of deep-tissue biological events. Thus, combination of these imaging modalities will provide synergistic benefits to facilitate more accurate disease diagnosis and longitudinal therapeutic response assessment.

PET (SPECT)/MRI

Since the debut of PET/MRI instruments (69), significant research interests have been devoted in this area. Three types of nanomaterials are useful for PET (SPECT)/MRI: radioactive magnetic iron oxide nanoparticles (IONPs), gadolinium (Gd)-containing nanomaterials, and manganese (Mn)-containing nanomaterials. The applications of radiolabeled IONPs in imaging applications (particularly PET/MRI and SPECT/MRI) have already been elucidated (70).

Compared with IONPs, Gd-containing nanomaterials are more preferred choice for PET (SPECT)/MRI applications since they are optimal T_1 contrast agents (positive contrast). As optimal image contrast agents, the applications of gadolinium oxide nanoparticles in PET/MRI has been reviewed recently (71). Maintaining the material integrity and preventing Gd dissociation are the main themes for successful imaging with Gd-containing nanomaterials. In an early report, ^{18}F-labeled, Gd-doped $NaYF_4$ nanophosphors were developed possessing PET, MRI, and upconversion luminescent properties (72). It showed a good paramagnetic longitudinal relaxivity and strong radiochemical stability (via strong interaction between Y and ^{18}F). From cells and tissue slide studies, these ^{18}F-labeled $NaYF_4$ nanophosphors could produce good contrast enhancement in PET/MRI. More

recently, ^{64}Cu-labeled and Eu-doped $GdVO_4$ nanosheets (NSs) were fabricated with radioactivity, fluorescence, and paramagnetic properties. The carboxyl-functionalized $GdVO_4$ NSs were further modified by DOTA for ^{64}Cu labeling and Asp-Gly-Glu-Ala (DGEA) peptide for integrin $\alpha_2\beta_1$ targeting (73). ^{64}Cu-DOTA-$GdVO_4$:Eu-DGEA demonstrated good accumulation in PC-3 tumor (integrin α_2,β_1^+) in vivo, confirmed by PET and T_1-weighted MRI.

As a well-known accommodating vector for Gd with good biocompatibility, fullerene can be combined with radionuclides to produce PET (SPECT)/MRI probes with good clinical future (74), although more research attention should be devoted to this type of application. A PET/MRI probe based on ^{124}I labeled $Gd_3N@C_{80}$ fullerene derivate was developed to avoid potential Gd leakage by caging the gadolinium ions firmly inside the fullerene structure (75). Not only can this biocompatible $Gd_3N@C_{80}$ be used as a T^1-weighted MRI agent and PET probe, it can also serve as a “radical sponge” to ameliorate inflammatory responses. Gd-containing organic nanomaterials were also appealing choices as PET/MRI contrast agents. For example, Gdcontaining liposome (via DTPA coordination) was labeled with ^{89}Zr by lipid membrane adsorption (76). By coupling with a SSTR2-targeted peptide, accumulation in $SSTR2^+$ tumors was more obvious compared with those in $SSTR2^-$tumors. Despite the popularity of Gd-containing nanomaterials, manipulating Gd complexes inevitably changes their behavior with respect to Gd release and relaxivity. This has also be taken into serious consideration during the design of Gd-based nanomaterials.

Excellent T_1 shortening characteristics qualify manganese for MRI applications while in vivo toxicity is the primary reason which hampers this otherwise useful contrast agent (77). Unlike gadolinium, an effective chelating agent for manganese with satisfactory in vivo stability has not been identified. Incorporation of manganese into stable nanostructures can provide new opportunities for imaging applications with manganese. Surprisingly, the research effort devoted on manganese-containing radio-nanomaterials is quite limited. To the best of our knowledge, only one existing report has used ^{64}Cu-labeled, human serum albumin (HSA) coated MnO nanoparticles for PET/MRI of glioblastoma (78). The coating of HSA in this report can boost material solubility and r_1 relaxivity. These ^{64}Cu-labeled MnO@HSA nanoparticles possessed good physiological stability, optimal distribution profile, and superior T_1 contrast. Good tumor delineation has been achieved with ^{64}Cu-labeled MnO@HSA in both PET and MRI. There are plenty of opportunities ahead for manganese-containing nanomaterials to be used in PET/MRI studies, since the production of ^{52}Mn ($t_{1/2}$ =5.6 days) has been optimized for PET applications (79).

PET (SPECT)/optical imaging

For radio-nanomaterials to be used for PET (SPECT)/ optical imaging, the material should either possess intrinsic optical emissions (fluorescence, photoacoustic signals, or Raman emissions), or be labeled by both a radioisotope and an optical emitter. With tunable fluorescence emission, QDs have a wide applicability in PET/fluorescence imaging. In one study, a dual receptor-targeting PET/NIRF probe was developed from QDs by further modification with β-Glu-RGD-BBN (BBN stands for bombesin) peptides and ^{18}F (80). QD-RGD-BBN exhibited strong NIRF emission with the maximum fluorescence wavelength at

705 nm. The functionalized QD probe has great potential as a universal dual-targeting probe for detecting tumors in living subjects with improved tumor-targeting efficacy.

Post-synthesis incorporation of both optical emitters and radioisotopes are most prevalent to produce PET/ optical imaging-suited nanomaterials. For example, MSNs conjugated with ^{64}Cu, 800 CW (a NIRF dye), and a monoclonal antibody against tumor vasculature, were adopted for PET/NIRF imaging of 4T1 breast tumors in one study (81). Good tumor targeting efficacy and specificity in tumor-bearing mice was achieved for these ^{64}Cu-labeled MSNs. A lot of attentions have been devoted on ultra-small silica-based Cornell dots (C-dots). C-dots are the first PET/fluorescence nano-probe that entered clinical testing. After conjugation with ^{124}I, an NIRF fluorophore (Cy5), and RGD peptide, C-dots were used for imaging of melanoma metastasis with improved SLN localization and retention, target-to-background ratios, and fast clearance from the body (primarily from renal pathways) (82). The specificity of this C-Dots platform, when compared with ^{18}F-FDG, for metastasis/ inflammation discrimination, was also satisfactory in the setting of surgery and therapeutic intervention. These radiolabeled C-dots were later used in a first-in-human clinical trial for lesion detection, cancer staging, and treatment management of patients with metastatic melanoma (Figure 4A) (83). ^{124}I-RGD-C-dots(Cy5) exhibited superior in vivo stability, good tolerance in patients, and sensitive detection of small metastatic lesions. Silica-based hybrid nanostructures are another category of PET/fluorescence contrast agents. For example, PAMAM-coated silica nanoparticles loaded with ^{99m}Tc and indocyanine green (ICG) were used for SLN mapping (85). NIR fluorescence imaging provided realtime clear fluorescent images of the lymph nodes with anatomical resolution. Although further studies are needed to determine the appropriate dose of the dual-imaging nanoparticle probe for effective sensitivity and safety, the results acquired in this study confirmed the value of this hybrid nanostructure for sentinel lymph node biopsy.

Photoacoustic imaging (PAI), based on the photoacoustic effect, is another attractive optical imaging technique with good resolution and contrast, portable instrumentation, and the ability to partially quantify the signal (86). PAI has been applied to the imaging of cancer, neurological disorders, vasculature function, and gene expression, among others. A ^{64}Cu-labeled, anisotropic branched gold nanomaterial (Au-tripod) was proved to be useful to generate good contrast in PET/PAI (87). Linear correlation between PAI signals and Au-tripods concentration was confirmed in vivo. Intravenous administration of ^{64}Cu-labeled, RGD peptide conjugated Au-tripods (RGD-Au-tripods) to U87MG tumor-bearing mice showed PAI contrast in tumors almost three-fold higher than for the blocking group, and PAI results correlated well with corresponding PET images. Melanin nanoparticle (MNP) was another attractive choice with unique photoacoustic property and natural binding ability with metal ions (e.g. ^{64}Cu), which enables them to be used as PET/PAI agents. With further conjugation of RGD peptide, ^{64}Cu-MNPs demonstrated potent accumulation in U87MG tumor, and this observation validated the value of MNPs as a theranostic platform for potential clinical translation (88). This radiolabeled MNPs can also be used as a PET/PAI guidable drug delivery platform in living mice (89). With apofer-ritin conjugation for transferrin receptor 1 (TfR1) targeting, ^{64}Cu-MNPs showed excellent stability and presented good tumor uptake and high tumor contrast in HT29 tumor (TfR1^{+}) with significantly lower accumulation in HepG2 (TfR1^{-}).

Multimodal imaging (with more than two modalities)

Nanoplatforms that combine more than two different imaging modalities have come into a research focus (90, 91). To achieve this, nanomaterials used are usually in a hybrid structure or a core/shell architecture to embrace more contrast capacity from different components (92–94).

A MRI/PET/fluorescence probe based the integration of IONP and UCNP was developed recently (95). The nanoparticles are composed of a core/shell Fe_3O_4@$NaYF_4$ nanoparticles with different metal ions doped (Yb, Er, Tm, etc.). With the stabilization from polyethylene glycol, the obtained nanoparticles showed high transverse relaxivity (r_2), good radiolabel stability, and strong upconversion luminescence. LNs in live mice could be clearly visualized by using ^{18}F labeled Fe_3O_4@$NaYF_4$ (Yb, Tm) nanoparticles in PET, MRI, and up-conversional luminescence (UCL). With a similar design, hybrid gold-IONP nanoparticles were made, in which IONPs worked as a T_2 MRI contrast agent, and the gold component acted as a strong fluorescence emitter and functionalization site [modified with 1,4,7-triazacyclononane-1,4,7-trisacetic acid (NOTA) for ^{64}Cu labeling] (92). Anti-EGFR affibody was also included to provide tumor targeting capabilities. As expected, the gold-IONP platform gave very sharp tumor contrast in PET, MRI, and fluorescence imaging. More recently, IONPs were assembled on the surface of two-dimensional MoS_2 nanosheets, forming MoS_2-IONP nanocomposites, which were then modified with PEG. ^{64}Cu could be adsorbed on the surface of MoS_2 without a chelator to enable PET imaging. The strong NIR emission and paramagnetic signals of MoS_2-IONP-PEG could also be utilized for PAI and MRI. Under the guidance by such triple-modal imaging, efficient tumor retention of MoS_2-IONP-PEG was confirmed, and effective tumor ablation was achieved in an image guidable manner in vivo. The same research group conducted hexamodal imaging using porphyrin-phospholipids coated UCNP (PoP-UCNP) (84). To more fully utilize the imaging capacity of this nanomaterial, it was characterized in vitro and in vivo for imaging via fluorescence, UCL, PET, CT, Cerenkov luminescence, and PAI (Figure 4B).

Therapeutic applications

Radiation therapy

Radio-nanomaterials were frequently used for delivering therapeutic isotopes to desired disease sites. The primary goal is to maximize the radiation dose to given cell population while decrease the radiation to normal tissues. Two types of isotopes are primarily used for therapeutic applications with radio-nanomaterials: α-emitters, and β-emitters.

β-emitter loaded radio-nanomaterials

β emitting radio-nuclides have found widespread use in cancer therapy due to their good availability and low production cost (96). Three β emitters are primarily used for production of radio-nanomaterials, namely, lutethium-177 (^{177}Lu), yttrium-90 (^{90}Y), and rhenium-188 (^{188}Re).

^{177}Lu

As a therapeutic isotope, ^{177}Lu emits β-particles (E_β =0.50 MeV, $t_{1/2}$=6.73 days) with moderate energy and a maximum travel range of 2 mm in tissues. AuNPs were radiolabeled with ^{177}Lu via DOTA and attached to RGD for targeting of integrin $\alpha_v\beta_3$ in the C6 glioma ($\alpha_v\beta_3^+$) (97). The therapeutic response of ^{177}Lu-AuNP-RGD was compared with that of ^{177}Lu-AuNP or ^{177}Lu-RGD. In this study, ^{177}Lu-AuNP-RGD delivered the highest tumor radiation absorbed dose (63.8±7.9 Gy) and triggered observable tumor regression. There was low uptake in non-target organs and no evidence of renal toxicity. More recently, ^{177}Lu-conjugated AuNPs were attached to panitumumab, an antibody against EGFR, and able to deliver even higher radiation dose (73.2±6.7 Gy) to breast tumors (Figure 5A) (98). To further increase the loading efficiency of ^{177}Lu onto nanomaterials, first (G1-) or fourth (G4-) generation PAMAM dendrimer were both used as the delivery vectors (100). It was shown that the G1- and G4-dendrimer conjugates, modified in average with 7.5 or 57 ^{177}Lu chelating units, respectively, can be labeled with ^{177}Lu with a significantly improved specific activity and radiochemical purity. G1-dendrimer conjugate demonstrated faster clearance in normal organs.

^{90}Y is a high energy β-emitter with a decay half-life of 64.1 h and E_β of 2.27 MeV, which can affect tumor cells up to a maximum depth of 11 mm in the soft tissue. Recently, ^{90}Y labeled N-(2-hydroxypropyl) methacrylamide (HPMA) nanoparticle was developed and its treatment efficacy was evaluated in prostate tumor (DU145) bearing mice (101). HPMA copolymer-DOTA conjugates demonstrated efficient labeling and stability for ^{90}Y and a marked accumulation of these radiolabeled copolymers was observed within prostate tumors. Histological analysis confirmed treatment efficacy and safety.

The relatively high energy from ^{90}Y requires more careful design of delivering method to limit its radiation to surrounding healthy tissues. In a clinical scenario, usually only several radioactive atoms (e.g. ^{90}Y) are linked to a targeting ligand (e.g. an antibody) and the deposited dose is often insufficient to eradicate solid tumors or tumors with radiation resistance. By replacing the single radionuclide by a radioactive nanoparticle containing hundreds of radioactive atoms, increased radiation dose can be delivered inside tumors. A study confirmed the benefit from $^{90}Y_2O_3$ nanoparticles for this application (102).

^{188}Re

Rhenium-188 is one of the most readily available generator-derived and useful radionuclides emitting β particles (2.12 MeV, 71.1% and 1.965 MeV, 25.6%, $t_{1/2}$=17 h) and gamma photons (155 keV, for imaging applications). The ^{188}W/^{188}Re generator is a good source for the long term (4–6 months) continuous availability of no-carrieradded ^{188}Re for radionuclide therapy (103). ^{188}Re-labeled magnetic nanoparticles (functionalized with albumin) were also loaded with cisplatin, and these nanoparticles could provide triple killing effects via hyperthermal therapy, chemotherapy, and radiotherapy (104). In vivo studies in tumor-bearing mice revealed that tumor uptake of these ^{188}Re-labeled magnetic albumin nanoparticles increased gradually after injection, peaked at 8 h and decreased gradually over time. This study confirmed the potential of ^{188}Re-labeled nanomaterials for tumor treatment, but until 2 years later the same group released their findings with the same material on

ovarian tumor treatment (105). Acquired results indicated that the combination of magnetic induced hyperthermia, chemotherapy and targeted radionuclide of radiation exposure could effectively inhibit the growth of ovarian cancer. In addition, G5 PAMAM dendrimer was radiolabeled with ^{188}Re, potentially useful for boosting isotope loading and facilitating subsequent functionalization (106).

Some unconventional β-emitting isotopes were also used for radio-nanomaterial production including ^{67}Ga (107), ^{166}Ho (108), and ^{198}Au (109). The incorporation chemistry and therapeutic application is very similar to what we have discussed above.

α-emitter loaded radio-nanomaterials

Compared with a variety of isotope choices of β-emitters, therapeutic application of α-emitter loaded nanomaterials is at a relatively preliminary stage. The smaller travel range of a-particles demands more precise delivery of radio-nanomaterials (110). The major challenge with α-emitter radiotherapies is that traditional chelating moieties are unable to sequester all the radioactive daughters, and this “detachment” can pose toxicity to healthy tissue. To provide more strict control of daughter radioisotopes, different methods have been proposed.

A number of targeted alpha therapy (TAT) agents based on the single α-emitting radionuclides ^{211}At (t =7.2 h), ^{213}Bi (t =46 months), ^{212}Pb (t =10.6 h), and ^{212}Bi (t =61 months) have been developed and showed promise in pre-clinical and clinical trials (111). The therapeutic efficacy of TAT could, however, be further enhanced by use of in vivo a-generator radionuclides like actinium-225 (^{225}Ac). ^{225}Ac can produce 4 net a-particles during its decay, dramatically amplifying the radiation dose delivered to the target (112). Moreover, the longer half-life of ^{225}Ac ($t_{1/2}$= 10 dsay) reduces activity loss during radiopharmaceutical production and allows longer time for localization of antibodies to the target sites. Radio-nanomaterials we mentioned in this section are primarily based on ^{225}Ac incorporation.

For effective TAT with ^{225}Ac, daughter radioisotopes (i.e. ^{221}Fr, ^{217}At, ^{213}Bi, and ^{209}Tl, Figure 5B) from the parent emissions should be sufficiently stable in the nanomaterials as the recoil energy of the ^{225}Ac daughters following α-decay can compromise metalligand bond used to stabilize ^{225}Ac. To solve this dilemma, a multilayered nanoparticle based on the structure of $La_{0.5}$ $Gd_{0.5}$ (^{225}Ac) PO_4@ $GdPO_4$@Au was used to constrain the decay daughters of ^{225}Ac (99). The stability of ^{225}Ac on these multi-shell nanoparticles was sufficiently high, and these nanoparticles demonstrated good receptor targeting efficacy after conjugation of an antibody (Figure 5B), which was monitored by SPECT/CT. Similarly structured layered nanoparticles were used in another study for treatment of lung tumors in mice (113). Retention of daughter ^{213}Bi in lung was about 90% at 24 h post-injection. Treatment of mice with lung-targeted ^{225}Ac NP significantly reduced EMT-6 lung colonies. Single-walled carbon nanotubes (SWNTs) was another useful carrier to bring ^{225}Ac into therapeutic applications (114). After loading of both ^{225}Ac and Gd^{3+} via bath sonication, the ^{225}Ac@GNTs were tested for stability against heat, time, and human serum. SWNTs could successfully sequester ^{225}Ac in the presence of Gd^{3+}, rendering ^{225}Ac@GNTs candidates for delivery of ^{225}Ac at higher concentrations.

Combinational therapies

Due to the evolving nature of cancer, monotherapies rarely catch up with the disease progression, especially for cancer. By tackling multiple targets, combinatorial treatments aim to improve the therapeutic index either through increased efficacy and overcoming resistance or through similar efficacy with reduced systemic toxicity. Most importantly, the combination of multiple therapeutic agents must generate a synergistic effect, ideally at lower doses than typical doses of each individual compound (115). The aforementioned ^{188}Re-containing, cisplatinloaded magnetic nanoparticles were good examples for combinational radio-/chemo- therapies (104, 105). Moreover, ^{90}Y-labeled albumin microspheres encapsulated with magnetite nanoparticles have been investigated for possible applications as a bimodal radionuclide-hyperthermia cancer therapy agent (116). In a later study, IONPs were also used to load ^{90}Y, functionalized with PEG (117). With reproducible high radiolabeling yield (>97%) labeling and good stability, these ^{90}Y-IONPs are also suitable candidates for MRI-magnetic hyperthermia and regional radiotherapy. Despite the foreseeable benefits of combinational therapy, the effort devoted in this area is very limited, and in some situation, the loaded isotope did not seem to play a synergistic role with other therapeutic elements. Another very unique nanomaterial type for combinational therapeutic application is boron-containing/enriched nanocomposites, which can emit α-particles after absorbing slow neutrons, although they are not radioactive before neutron activation (118). The nuclear capture reaction concept is known as boron neutron capture therapy (BNCT). BNCT is a potentially promising treatment for malignant brain tumors as well as other cancers, despite the fact that neutron sources may not always be available.

Summary and future perspectives

Employing nanotechnology in delivery of diagnostic/therapeutic agents offers significant advantages, including normalized pharmacokinetics and pharmacodynamics, sustained bioavailability, targeted accumulation, and controllable drug release. Radio-nanomaterials, with synergistic integration of physical/chemical/functional properties from the material(s) and the isotope(s), are important players for different biomedical applications (Table 2). There are two critical composing elements for a radioactive nanomaterial, i.e. the radioisotope, and the nanomaterial. To make the radioactive nanomaterial readily applicable for different biomedical applications, the suitable selection of both components should be synergistic. On the one hand, incorporation of radioisotope(s) bestows extra tracking/therapeutic ability to the nanomaterial which cannot be acquired by loading of other cargos. On the other hand, the utilization of suitable nanomaterials may serve as an isotope carrier and enable some unconventional isotopes to be used in specific biomedical applications which might otherwise be very difficult to achieve, for example, gemanium-69 (^{69}Ge) (9), or sodium-22 (^{22}Na) (10).

The ability to track the kinetics of nanomaterials in humans and research animals on a whole body basis can provide invaluable information to researchers for development of efficient diagnostic or therapeutic agents. The attachment of radionuclides to nanomaterials can facilitate the tracking of nanomaterials in vivo and help to clarify their pharmacokinetic behaviors (stability, organ absorption/distribution, clearance, etc.). Different imaging

"labels" can be integrated into a single nanoplatform for combining the strengths of different imaging modalities, which can synergistically improve the overall value of imaging in the context of basic research or patient care. In addition, nanomaterials with appropriate functionalization can evade attack from the immune system and thus create prolonged imaging time (11). Moreover, as most nanomaterials have large surface areas which result in superior cargo accommodating capacity, they can help to increase local imaging contrast in selected areas. In addition, loading of imaging labels (isotopes/ fluorophores, etc.) in nanomaterials can cause alterations of the in vivo pharmacokinetics of the labels, which can be tunable for image optimization in most cases.

One of the major challenges associated with radionuclide therapies is the inherent toxicity from the radiation damage to normal, healthy tissues. For example, although β emitting radionuclides have found widespread use in cancer therapy, the long travel range of β particles (e.g. 1.5 mm for ^{177}Lu and 12 mm for ^{90}Y) tends to pose damage to the surrounding tissues. Radiotherapies based on α particle emission can serve as a promising alternative since α particles deposit all of their energy within a few cell diameters (50–100 μm), thus accurate delivery of α emitters (and potentially daughter isotopes after decay) to the diseased sites is the prerequisite for effective cell killing. For both α and β emitters, incorporation into nanomaterials can increase effective dose delivered to diseased locations (particularly cancer). With or without the company of an "active targeting" ligand, radio-nanomaterials can alter the pharmacokinetics of the loaded α-/β- emitters, usually resulting in decreased toxicity. Significantly more research efforts will be devoted to prepare nanomaterials with better radiochemical stability, more optimal isotope loading efficiency, and more beneficial clearance profile.

Using one drug for cancer therapy is usually considered as ineffective: tackling on a specific target pathway often result in the activation of more pathogenic pathways as a compensation (119, 120). Therefore, combinatorial therapies using multiple therapeutic agents together for generating synergistic effects is a logical approach to combat cancer since they can respond to the dynamic nature of cancer during the treatment. By using radio-nanomaterials, multi-dimensional therapeutic options can be tested easily for a specific cancer type or in a given individual. Keep in mind that it is indispensable to ensure that these treatments are synergistic and complementary. The potential adverse effects from radio-nanomaterials need to be also considered when incorporating other therapeutic elements. Finally, the radio-nanomaterials usable for combinational therapy should not involve complex manufacturing process, and should be highly assessable to the majority of the research community and clinics.

Selection of radio-nanomaterial candidates to be eventually useful in clinics is extremely challenging, and the balance between cost and benefit must be judiciously mapped out. Radio-nanomaterials offer researchers and clinicians new tools to visualize the fate of these materials, evaluate their interaction for a given disease, and provide improvement to current disease therapies. Looking forward, these radio-nanomaterials are expected to play an even more important role in shaping the future of nanotheranostics.

Acknowledgments

This work was supported, in part, by the National Institutes of Health (NIBIB/NCI R01CA169365, P30CA014520), the American Cancer Society (125246-RSG-13-099-01-CCE), and the Pardee Foundation Grant (to H.H.).

References

1. Cole JT, Holland NB. Multifunctional nanoparticles for use in theranostic applications. Drug Deliv Transl Res. 2015; 5:295–309. [PubMed: 25787729]
2. Chen F, Ehlerding EB, Cai W. Theranostic nanoparticles. J Nucl Med. 2014; 55:1919–1922. [PubMed: 25413134]
3. He C, Lin W. Hybrid nanoparticles for cancer imaging and therapy. Cancer Treat Res. 2015; 166:173–192. [PubMed: 25895869]
4. Soni G, Yadav KS. Applications of nanoparticles in treatment and diagnosis of leukemia. Mater Sci Eng C Mater Biol Appl. 2015; 47:156–164. [PubMed: 25492184]
5. Cheng Z, Al Zaki A, Hui JZ, Muzykantov VR, Tsourkas A. Multifunctional nanoparticles: cost versus benefit of adding targeting and imaging capabilities. Science. 2012; 338:903–910. [PubMed: 23161990]
6. Kharisov BI, Kharissova OV, Berdonosov SS. Radioactive nanoparticles and their main applications: recent advances. Recent Pat Nanotechnol. 2014; 8:79–96. [PubMed: 24962376]
7. Chen F, Ellison PA, Lewis CM, Hong H, Zhang Y, Shi S, et al. Chelator-free synthesis of a dual-modality PET/MRI agent. Angew Chem Int Ed Engl. 2013; 52:13319–13323. [PubMed: 24166933]
8. Ellison PA, Barnhart TE, Chen F, Hong H, Zhang Y, Theuer CP, et al. High yield production and radiochemical isolation of isotopically pure arsenic-72 and novel radioarsenic labeling strategies for the development of theranostic radiopharmaceuticals. Bioconjug Chem. 2016; 27:179–188. [PubMed: 26646989]
9. Chakravarty R, Valdovinos HF, Chen F, Lewis CM, Ellison PA, Luo H, et al. Intrinsically germanium-69-labeled iron oxide nanoparticles: synthesis and in-vivo dual-modality PET/MR imaging. Adv Mater. 2014; 26:5119–5123. [PubMed: 24944166]
10. Al Faraj A, Alotaibi B, Shaik AP, Shamma KZ, Al Jammaz I, Gerl J. Sodium-22-radiolabeled silica nanoparticles as new radiotracer for biomedical applications: in vivo positron emission tomography imaging, biodistribution, and biocompatibility. Int J Nanomedicine. 2015; 10:6293–6302. [PubMed: 26504381]
11. Sun X, Cai W, Chen X. Positron emission tomography imaging using radiolabeled inorganic nanomaterials. Acc Chem Res. 2015; 48:286–294. [PubMed: 25635467]
12. Volotskova O, Sun C, Stafford JH, Koh AL, Ma X, Cheng Z, et al. Efficient radioisotope energy transfer by gold nanoclusters for molecular imaging. Small. 2015; 11:4002–4008. [PubMed: 25973916]
13. Hughes MF, Long TC, Boyes WK, Ramabhadran R. Whole-body retention and distribution of orally administered radiolabelled zerovalent iron nanoparticles in mice. Nanotoxicology. 2013; 7:1064–1069. [PubMed: 22662881]
14. Perez-Campana C, Gomez-Vallejo V, Puigivila M, Martin A, Calvo-Fernandez T, Moya SE, et al. Biodistribution of different sized nanoparticles assessed by positron emission tomography: a general strategy for direct activation of metal oxide particles. ACS Nano. 2013; 7:3498–3505. [PubMed: 23473535]
15. Black KC, Wang Y, Luehmann HP, Cai X, Xing W, Pang B, et al. Radioactive ^{198}Au-doped nanostructures with different shapes for in vivo analyses of their biodistribution, tumor uptake, and intratumoral distribution. ACS Nano. 2014; 8:4385–4394. [PubMed: 24766522]
16. Wang H, Kumar R, Nagesha D, Duclos RI Jr, Sridhar S, Gatley SJ. Integrity of ^{111}In-radiolabeled superparamagnetic iron oxide nanoparticles in the mouse. Nucl Med Biol. 2015; 42:65–70. [PubMed: 25277378]
17. Benezra M, Hambardzumyan D, Penate-Medina O, Veach DR, Pillarsetty N, Smith-Jones P, et al. Fluorine-labeled dasatinib nanoformulations as targeted molecular imaging probes in a PDGFB-driven murine glioblastoma model. Neoplasia. 2012; 14:1132–1143. [PubMed: 23308046]

18. Wennerberg A, Jimbo R, Allard S, Skarnemark G, Andersson M. In vivo stability of hydroxyapatite nanoparticles coated on titanium implant surfaces. Int J Oral Maxillofac Implants. 2011; 26:1161–1166. [PubMed: 22167419]
19. Sun Y, Liu Q, Peng J, Feng W, Zhang Y, Yang P, et al. Radioisotope post-labeling upconversion nanophosphors for in vivo quantitative tracking. Biomaterials. 2013; 34:2289–2295. [PubMed: 23274071]
20. Yang Y, Sun Y, Cao T, Peng J, Liu Y, Wu Y, et al. Hydrothermal synthesis of $NaLuF_4$:^{153}Sm,Yb,Tm nanoparticles and their application in dual-modality upconversion luminescence and SPECT bioimaging. Biomaterials. 2013; 34:774–783. [PubMed: 23117216]
21. Sanchez-Martinez M, da Costa Martins R, Quincoces G, Gamazo C, Caicedo C, Irache JM, et al. Radiolabeling and biodistribution studies of polymeric nanoparticles as adjuvants for ocular vaccination against brucellosis. Rev Esp Med Nucl Imagen Mol. 2013; 32:92–97. [PubMed: 23332663]
22. Woods A, Patel A, Spina D, Riffo-Vasquez Y, Babin-Morgan A, de Rosales RT, et al. In vivo biocompatibility, clearance, and biodistribution of albumin vehicles for pulmonary drug delivery. J Control Release. 2015; 210:1–9. [PubMed: 25980621]
23. Lee CM, Jeong HJ, Kim DW, Sohn MH, Lim ST. The effect of fluorination of zinc oxide nanoparticles on evaluation of their biodistribution after oral administration. Nanotechnology. 2012; 23:205102. [PubMed: 22543822]
24. Yeh TK, Chen JK, Lin CH, Yang MH, Yang CS, Chou FI, et al. Kinetics and tissue distribution of neutron-activated zinc oxide nanoparticles and zinc nitrate in mice: effects of size and particulate nature. Nanotechnology. 2012; 23:085102. [PubMed: 22293282]
25. Lin YY, Li JJ, Chang CH, Lu YC, Hwang JJ, Tseng YL, et al. Evaluation of pharmacokinetics of ^{111}In-labeled VNB-PEGylated liposomes after intraperitoneal and intravenous administration in a tumor/ascites mouse model. Cancer Biother Radiopharm. 2009; 24:453–460. [PubMed: 19694580]
26. Xie H, Goins B, Bao A, Wang ZJ, Phillips WT. Effect of intratumoral administration on biodistribution of ^{64}Cu-labeled nanoshells. Int J Nanomedicine. 2012; 7:2227–2238. [PubMed: 22619558]
27. Tian M, Lu W, Zhang R, Xiong C, Ensor J, Nazario J, et al. Tumor uptake of hollow gold nanospheres after intravenous and intra-arterial injection: PET/CT study in a rabbit VX2 liver cancer model. Mol Imaging Biol. 2013; 15:614–624. [PubMed: 23608932]
28. Beloqui A, Solinis MA, Delgado A, Evora C, del Pozo-Rodriguez A, Rodriguez-Gascon A. Biodistribution of nanostructured lipid carriers (NLCs) after intravenous administration to rats: influence of technological factors. Eur J Pharm Biopharm. 2013; 84:309–314. [PubMed: 23461861]
29. Chakravarty R, Hong H, Cai W. Positron emission tomography imageguided drug delivery: current status and future perspectives. Mol Pharm. 2014; 11:3777–3797. [PubMed: 24865108]
30. Chen F, Goel S, Valdovinos HF, Luo H, Hernandez R, Barnhart TE, et al. In vivo integrity and biological fate of chelator-free zirconium-89-labeled mesoporous silica nanoparticles. ACS Nano. 2015; 9:7950–7959. [PubMed: 26213260]
31. Zhao Y, Sultan D, Detering L, Cho S, Sun G, Pierce R, et al. Cop-per-64-alloyed gold nanoparticles for cancer imaging: improved radiolabel stability and diagnostic accuracy. Angew Chem Int Ed Engl. 2014; 53:156–159. [PubMed: 24272951]
32. Zeng J, Jia B, Qiao R, Wang C, Jing L, Wang F, et al. In situ ^{111}In-doping for achieving biocompatible and non-leachable ^{111}In-labeled Fe_3O_4 nanoparticles. Chem Commun (Camb). 2014; 50:2170–2172. [PubMed: 24430864]
33. Khawar IA, Kim JH, Kuh HJ. Improving drug delivery to solid tumors: priming the tumor microenvironment. J Control Release. 2015; 201:78–89. [PubMed: 25526702]
34. Sheng Y, Liao LD, Thakor NV, Tan MC. Nanoparticles for molecular imaging. J Biomed Nanotechnol. 2014; 10:2641–2676. [PubMed: 25992413]
35. Srivatsan A, Chen X. Recent advances in nanoparticle-based nuclear imaging of cancers. Adv Cancer Res. 2014; 124:83–129. [PubMed: 25287687]

36. Albernaz Mde S, Ospina CA, Rossi AM, Santos-Oliveira R. Radiolabelled nanohydroxyapatite with ^{99m}Tc: perspectives to nanoradiopharmaceuticals construction. Artif Cells Nanomed Biotechnol. 2014; 42:88–91. [PubMed: 23586417]
37. Sakurai Y, Kajimoto K, Hatakeyama H, Harashima H. Advances in an active and passive targeting to tumor and adipose tissues. Expert Opin Drug Deliv. 2015; 12:41–52. [PubMed: 25376864]
38. Hong H, Zhang Y, Engle JW, Nayak TR, Theuer CP, Nickles RJ, et al. In vivo targeting and positron emission tomography imaging of tumor vasculature with ^{66}Galabeled nanographene. Biomaterials. 2012; 33:4147–4156. [PubMed: 22386918]
39. Hong H, Yang K, Zhang Y, Engle JW, Feng L, Yang Y, et al. In vivo targeting and imaging of tumor vasculature with radiolabeled, antibody-conjugated nanographene. ACS Nano. 2012; 6:2361–2370. [PubMed: 22339280]
40. Shi S, Yang K, Hong H, Valdovinos HF, Nayak TR, Zhang Y, et al. Tumor vasculature targeting and imaging in living mice with reduced graphene oxide. Biomaterials. 2013; 34:3002–3009. [PubMed: 23374706]
41. Cornelissen B, Able S, Kersemans V, Waghorn PA, Myhra S, Jurkshat K, et al. Nanographene oxide-based radioimmunoconstructs for in vivo targeting and SPECT imaging of HER2-positive tumors. Biomaterials. 2013; 34:1146–1154. [PubMed: 23171545]
42. Chen F, Hong H, Shi S, Goel S, Valdovinos HF, Hernandez R, et al. Engineering of hollow mesoporous silica nanoparticles for remarkably enhanced tumor active targeting efficacy. Sci Rep. 2014; 4:5080. [PubMed: 24875656]
43. Perez-Medina C, Tang J, Abdel-Atti D, Hogstad B, Merad M, Fisher EA, et al. PET imaging of tumor-associated macrophages with ^{89}Zr-labeled high-density lipoprotein nanoparticles. J Nucl Med. 2015; 56:1272–1277. [PubMed: 26112022]
44. Chen F, Hong H, Zhang Y, Valdovinos HF, Shi S, Kwon GS, et al. In vivo tumor targeting and image-guided drug delivery with antibody-conjugated, radiolabeled mesoporous silica nanoparticles. ACS Nano. 2013; 7:9027–9039. [PubMed: 24083623]
45. Chen Y, Chen H, Shi J. In vivo bio-safety evaluations and diagnostic/therapeutic applications of chemically designed mesoporous silica nanoparticles. Adv Mater. 2013; 25:3144–3176. [PubMed: 23681931]
46. Zhu J, Chin J, Wangler C, Wangler B, Lennox RB, Schirrmacher R. Rapid ^{18}F-labeling and loading of PEGylated gold nanoparticles for in vivo applications. Bioconjug Chem. 2014; 25:1143–1150. [PubMed: 24807200]
47. Melancon MP, Zhou M, Zhang R, Xiong C, Allen P, Wen X, et al. Selective uptake and imaging of aptamer- and antibody-conjugated hollow nanospheres targeted to epidermal growth factor receptors overexpressed in head and neck cancer. ACS Nano. 2014; 8:4530–4538. [PubMed: 24754567]
48. Sun X, Huang X, Yan X, Wang Y, Guo J, Jacobson O, et al. Chelator-free ^{64}Cu-integrated gold nanomaterials for positron emission tomography imaging guided photothermal cancer therapy. ACS Nano. 2014; 8:8438–8446. [PubMed: 25019252]
49. Phillips WT, Goins BA, Bao A. Radioactive liposomes. Wiley Inter-discip Rev Nanomed Nanobiotechnol. 2009; 1:69–83.
50. Silindir M, Ozer AY, Erdogan S. The use and importance of liposomes in positron emission tomography. Drug Deliv. 2012; 19:68–80. [PubMed: 22211758]
51. Silindir M, Erdogan S, Ozer AY, Dogan AL, Tuncel M, Ugur O, et al. Nanosized multifunctional liposomes for tumor diagnosis and molecular imaging by SPECT/CT. J Liposome Res. 2013; 23:20–27. [PubMed: 23078019]
52. Rangger C, Helbok A, Sosabowski J, Kremser C, Koehler G, Prassl R, et al. Tumor targeting and imaging with dual-peptide conjugated multifunctional liposomal nanoparticles. Int J Nanomedicine. 2013; 8:4659–4671. [PubMed: 24353415]
53. Orocio-Rodriguez E, Ferro-Flores G, Santos-Cuevas CL, Ramirez Fde M, Ocampo-Garcia BE, Azorin-Vega E, et al. Two novel nanosized radiolabeled analogues of somatostatin for nuroendocrine tumor imaging. J Nanosci Nanotechnol. 2015; 15:4159–4169. [PubMed: 26369025]
54. Narunsky L, Oren R, Bochner F, Neeman M. Imaging aspects of the tumor stroma with therapeutic implications. Pharmacol Ther. 2014; 141:192–208. [PubMed: 24134903]

55. Li J, Zhuang Z, Jiang B, Zhao P, Lin C. Advances and perspectives in nanoprobes for noninvasive lymph node mapping. Nanomedicine (Lond). 2015; 10:1019–1036. [PubMed: 25867863]
56. Majmudar MD, Yoo J, Keliher EJ, Truelove JJ, Iwamoto Y, Sena B, et al. Polymeric nanoparticle PET/MR imaging allows macrophage detection in atherosclerotic plaques. Circ Res. 2013; 112:755–761. [PubMed: 23300273]
57. Luehmann HP, Pressly ED, Detering L, Wang C, Pierce R, Woodard PK, et al. PET/CT imaging of chemokine receptor CCR5 in vascular injury model using targeted nanoparticle. J Nucl Med. 2014; 55:629–634. [PubMed: 24591489]
58. Bogdanov AA Jr, Gupta S, Koshkina N, Corr SJ, Zhang S, Curley SA, et al. Gold nanoparticles stabilized with MPEG-grafted poly(l-lysine): in vitro and in vivo evaluation of a potential theranostic agent. Bioconjug Chem. 2015; 26:39–50. [PubMed: 25496453]
59. Hwang H, Kwon J, Oh PS, Lee TK, Na KS, Lee CM, et al. Peptide-loaded nanoparticles and radionuclide imaging for individualized treatment of myocardial ischemia. Radiology. 2014; 273:160–167. [PubMed: 24927328]
60. Peng J, Sun Y, Zhao L, Wu Y, Feng W, Gao Y, et al. Polyphosphoric acid capping radioactive/upconverting NaLuF4: Yb,Tm,153Sm nanoparticles for blood pool imaging in vivo. Biomaterials. 2013; 34:9535–9544. [PubMed: 24011713]
61. Frigell J, Garcia I, Gomez-Vallejo V, Llop J, Penades S. ^{68}Galabeled gold glyconanoparticles for exploring blood-brain barrier permeability: preparation, biodistribution studies, and improved brain uptake via neuropeptide conjugation. J Am Chem Soc. 2014; 136:449–457. [PubMed: 24320878]
62. Das S, Thorek DL, Grimm J. Cerenkov imaging. Adv Cancer Res. 2014; 124:213–234. [PubMed: 25287690]
63. Guo W, Sun X, Jacobson O, Yan X, Min K, Srivatsan A, et al. Intrinsically radioactive [^{64}Cu]CuInS/ZnS quantum dots for PET and optical imaging: improved radiochemical stability and controllable Cerenkov luminescence. ACS Nano. 2015; 9:488–495. [PubMed: 25549258]
64. Sun X, Huang X, Guo J, Zhu W, Ding Y, Niu G, et al. Self-illuminating ^{64}Cu-doped CdSe/ZnS nanocrystals for in vivo tumor imaging. J Am Chem Soc. 2014; 136:1706–1709. [PubMed: 24401138]
65. Kotagiri N, Niedzwiedzki DM, Ohara K, Achilefu S. Activatable probes based on distance-dependent luminescence associated with Cerenkov radiation. Angew Chem Int Ed Engl. 2013; 52:7756–7760. [PubMed: 23765506]
66. Wang Y, Liu Y, Luehmann H, Xia X, Wan D, Cutler C, et al. Radio-luminescent gold nanocages with controlled radioactivity for real-time in vivo imaging. Nano Lett. 2013; 13:581–585. [PubMed: 23360442]
67. Hu H, Huang P, Weiss OJ, Yan X, Yue X, Zhang MG, et al. PET and NIR optical imaging using self-illuminating ^{64}Cu-doped chelator-free gold nanoclusters. Biomaterials. 2014; 35:9868–9876. [PubMed: 25224367]
68. James ML, Gambhir SS. A molecular imaging primer: modalities, imaging agents, and applications. Physiol Rev. 2012; 92:897–965. [PubMed: 22535898]
69. Pichler BJ, Judenhofer MS, Catana C, Walton JH, Kneilling M, Nutt RE, et al. Performance test of an LSO-APD detector in a 7-T MRI scanner for simultaneous PET/MRI. J Nucl Med. 2006; 47:639–647. [PubMed: 16595498]
70. Ai F, Ferreira CA, Chen F, Cai W. Engineering of radiolabeled iron oxide nanoparticles for dual-modality imaging. Wiley Interdiscip Rev Nanomed Nanobiotechnol. 2015
71. Kim TJ, Chae KS, Chang Y, Lee GH. Gadolinium oxide nanoparticles as potential multimodal imaging and therapeutic agents. Curr Top Med Chem. 2013; 13:422–433. [PubMed: 23432005]
72. Zhou J, Yu M, Sun Y, Zhang X, Zhu X, Wu Z, et al. Fluorine-18-la-beled $Gd^{3+}/Yb^{3+}/Er^{3+}$ co-doped $NaYF_4$ nanophosphors for multimodality PET/MR/UCL imaging. Biomaterials. 2011; 32:1148–1156. [PubMed: 20965563]
73. Hu H, Li D, Liu S, Wang M, Moats R, Conti PS, et al. Integrin alpha2beta1 targeted $GdVO_4$:Eu ultrathin nanosheet for multimodal PET/MR imaging. Biomaterials. 2014; 35:8649–8658. [PubMed: 25043573]

74. Chen D, Dougherty CA, Zhu K, Hong H. Theranostic applications of carbon nanomaterials in cancer: focus on imaging and cargo delivery. J Control Release. 2015; 210:230–245. [PubMed: 25910580]
75. Luo J, Wilson JD, Zhang J, Hirsch JI, Dorn HC, Fatouros PP, et al. A dual PET/MR imaging nanoprobe: ^{124}I labeled $Gd_3N@C_{80}$. Appl Sci. 2012; 2:465–478.
76. Abou DS, Thorek DL, Ramos NN, Pinkse MW, Wolterbeek HT, Carlin SD, et al. ^{89}Zr-labeled paramagnetic octreotide-liposomes for PET-MR imaging of cancer. Pharm Res. 2013; 30:878–888. [PubMed: 23224977]
77. Crossgrove J, Zheng W. Manganese toxicity upon overexposure. NMR Biomed. 2004; 17:544–553. [PubMed: 15617053]
78. Huang J, Xie J, Chen K, Bu L, Lee S, Cheng Z, et al. HSA coated MnO nanoparticles with prominent MRI contrast for tumor imaging. Chem Commun (Camb). 2010; 46:6684–6686. [PubMed: 20730157]
79. Graves SA, Hernandez R, Fonslet J, England CG, Valdovinos HF, Ellison PA, et al. Novel preparation methods of ^{52}Mn for immun-oPET imaging. Bioconjug Chem. 2015; 26:2118–2124. [PubMed: 26317429]
80. Hu K, Wang H, Tang G, Huang T, Tang X, Liang X, et al. In vivo cancer dualtargeting and dualmodality imaging with functionalized quantum dots. J Nucl Med. 2015; 56:1278–1284. [PubMed: 26112023]
81. Chen F, Nayak TR, Goel S, Valdovinos HF, Hong H, Theuer CP, et al. In vivo tumor vasculature targeted PET/NIRF imaging with TRC105(Fab)-conjugated, duallabeled mesoporous silica nanoparticles. Mol Pharm. 2014; 11:4007–4014. [PubMed: 24937108]
82. Bradbury MS, Phillips E, Montero PH, Cheal SM, Stambuk H, Durack JC, et al. Clinically-translated silica nanoparticles as dual-modality cancer-targeted probes for image-guided surgery and interventions. Integrative Biology. 2013; 5:74–86. [PubMed: 23138852]
83. Phillips E, Penate-Medina O, Zanzonico PB, Carvajal RD, Mohan P, Ye Y, et al. Clinical translation of an ultrasmall inorganic optical-PET imaging nanoparticle probe. Sci Transl Med. 2014; 6:260ra149.
84. Rieffel J, Chen F, Kim J, Chen G, Shao W, Shao S, et al. Hexamodal imaging with porphyrin-phospholipid-coated upconversion nanoparticles. Adv Mater. 2015; 27:1785–1790. [PubMed: 25640213]
85. Tsuchimochi M, Hayama K, Toyama M, Sasagawa I, Tsubokawa N. Dual-modality imaging with ^{99m}Tc and fluorescent indocyanine green using surface-modified silica nanoparticles for biopsy of the sentinel lymph node: an animal study. EJNMMI Res. 2013; 3:33. [PubMed: 23618132]
86. Zhang Y, Hong H, Cai W. Photoacoustic imaging. Cold Spring Harb Protoc. 2011:2011. [PubMed: 21363959]
87. Cheng K, Kothapalli SR, Liu H, Koh AL, Jokerst JV, Jiang H, et al. Construction and validation of nano gold tripods for molecular imaging of living subjects. J Am Chem Soc. 2014; 136:3560–3571. [PubMed: 24495038]
88. Fan Q, Cheng K, Hu X, Ma X, Zhang R, Yang M, et al. Transferring biomarker into molecular probe: melanin nanoparticle as a naturally active platform for multimodality imaging. J Am Chem Soc. 2014; 136:15185–15194. [PubMed: 25292385]
89. Zhang R, Fan Q, Yang M, Cheng K, Lu X, Zhang L, et al. Engineering melanin nanoparticles as an efficient drug-delivery system for imaging-guided chemotherapy. Adv Mater. 2015; 27:5063–5069. [PubMed: 26222210]
90. Park JC, Yu MK, An GI, Park SI, Oh J, Kim HJ, et al. Facile preparation of a hybrid nanoprobe for triple-modality optical/ PET/MR imaging. Small. 2010; 6:2863–2868. [PubMed: 21104828]
91. Kang KW. Preliminary pre-clinical results and overview on PET/MRI/fluorescent molecular imaging. Open Nuclear Med J. 2010; 2:153–156.
92. Yang M, Cheng K, Qi S, Liu H, Jiang Y, Jiang H, et al. Affibody modified and radiolabeled goldiron oxide hetero-nanostructures for tumor PET, optical and MR imaging. Biomaterials. 2013; 34:2796–2806. [PubMed: 23343632]
93. Xie J, Chen K, Huang J, Lee S, Wang J, Gao J, et al. PET/NIRF/ MRI triple functional iron oxide nanoparticles. Biomaterials. 2010; 31:3016–3022. [PubMed: 20092887]

94. Huang X, Zhang F, Lee S, Swierczewska M, Kiesewetter DO, Lang L, et al. Long-term multimodal imaging of tumor draining sentinel lymph nodes using mesoporous silica-based nanoprobes. Biomaterials. 2012; 33:4370–4378. [PubMed: 22425023]

95. Cui X, Mathe D, Kovács N, Horváth I, Jauregui-Osoro M, Torres Martin de Rosales R, et al. Synthesis, characterization, and application of core-shell $Co_{0.16}Fe_{2.84}O_4$@ $NaYF_4$ (Yb, Er) and Fe_3O_4@ $NaYF_4$ (Yb, Tm) nanoparticle as trimodal (MRI, PET/SPECT, and optical) imaging agents. Bioconjug Chem. 2016; 27:319–328. [PubMed: 26172432]

96. Parus JL, Mikolajczak R. Beta-emitting radionuclides for peptide receptor radionuclide therapy. Curr Top Med Chem. 2012; 12:2686–2693. [PubMed: 23339764]

97. Vilchis-Juarez A, Ferro-Flores G, Santos-Cuevas C, Morales-Avila E, Ocampo-Garcia B, Diaz-Nieto L, et al. Molecular targeting radiotherapy with cyclo-RGDFK(C) peptides conjugated to ^{177}Lu-labeled gold nanoparticles in tumor-bearing mice. J Biomed Nanotechnol. 2014; 10:393–404. [PubMed: 24730235]

98. Yook S, Cai Z, Lu Y, Winnik MA, Pignol JP, Reilly RM. Radiation nanomedicine for EGFR-positive breast cancer: panitumumabmodified gold nanoparticles complexed to the beta-particle-emitter, ^{177}Lu. Mol Pharm. 2015; 12:3963–3972. [PubMed: 26402157]

99. McLaughlin MF, Woodward J, Boll RA, Wall JS, Rondinone AJ, Kennel SJ, et al. Gold coated lanthanide phosphate nanoparticles for targeted alpha generator radiotherapy. PLoS One. 2013; 8:e54531. [PubMed: 23349921]

100. Laznickova A, Biricova V, Laznicek M, Hermann P. Mono(pyridine-N-oxide) DOTA analog and its G1/G4-PAMAM dendrimer conjugates labeled with ^{177}Lu: radiolabeling and biodistribution studies. Appl Radiat Isot. 2014; 84:70–77. [PubMed: 24333746]

101. Buckway B, Frazier N, Gormley AJ, Ray A, Ghandehari H. Gold nanorod-mediated hyperthermia enhances the efficacy of HPMA copolymer-^{90}Y conjugates in treatment of prostate tumors. Nucl Med Biol. 2014; 41:282–289. [PubMed: 24461626]

102. Bouchat V, Nuttens VE, Michiels C, Masereel B, Feron O, Gallez B, et al. Radioimmunotherapy with radioactive nanoparticles: biological doses and treatment efficiency for vascularized tumors with or without a central hypoxic area. Med Phys. 2010; 37:1826–1839. [PubMed: 20443505]

103. Pillai MR, Dash A, Knapp FF Jr. Rhenium-188: availability from the ^{188}W/^{188}Re generator and status of current applications. Curr Radiopharm. 2012; 5:228–243. [PubMed: 22642385]

104. Tang QS, Chen DZ, Xue WQ, Xiang JY, Gong YC, Zhang L, et al. Preparation and biodistribution of 188Re-labeled folate conjugated human serum albumin magnetic cisplatin nanoparticles (^{188}Re-folate-CDDP/HSA MNPs) in vivo. Int J Nanomedicine. 2011; 6:3077–3085. [PubMed: 22163161]

105. Tang Q, Chen D. Study of the therapeutic effect of ^{188}Re labeled folate targeting albumin nanoparticle coupled with cis-diam-minedichloroplatinum cisplatin on human ovarian cancer. Biomed Mater Eng. 2014; 24:711–722. [PubMed: 24211956]

106. Cui W, Zhang Y, Xu X, Shen YM. Synthesis and ^{188}Re radiolabelling of dendrimer polyamide amine (PAMAM) folic acid conjugate. Med Chem. 2012; 8:727–731. [PubMed: 22548334]

107. Hosseini-Salekdeh SL, Jalilian AR, Yousefnia H, Shafaii K, Pouladian M, Mahmoudi M. Evaluation of radiogallium-labeled, folate-embedded superparamagnetic nanoparticles in fbrosarcoma-bearing mice. J Cancer Res Ther. 2012; 8:204–208. [PubMed: 22842362]

108. Munaweera I, Levesque-Bishop D, Shi Y, Di Pasqua AJ, Balkus KJ Jr. Radiotherapeutic bandage based on electrospun polyacrylonitrile containing holmium-166 iron garnet nanoparticles for the treatment of skin cancer. ACS Appl Mater Interfaces. 2014; 6:22250–22256. [PubMed: 25396281]

109. Shukla R, Chanda N, Zambre A, Upendran A, Katti K, Kulkarni RR, et al. Laminin receptor specific therapeutic gold nanoparticles (^{198}AuNP-EGCg) show efficacy in treating prostate cancer. Proc Natl Acad Sci USA. 2012; 109:12426–12431. [PubMed: 22802668]

110. Gudkov SV, Shilyagina NY, Vodeneev VA, Zvyagin AV. Targeted radionuclide therapy of human tumors. Int J Mol Sci. 2016:17.

111. Kim YS, Brechbiel MW. An overview of targeted alpha therapy. Tumour Biol. 2012; 33:573–590. [PubMed: 22143940]

112. Scheinberg DA, McDevitt MR. Actinium-225 in targeted alpha-particle therapeutic applications. Curr Radiopharm. 2011; 4:306–320. [PubMed: 22202153]

113. McLaughlin MF, Robertson D, Pevsner PH, Wall JS, Mirzadeh S, Kennel SJ. $LnPO_4$ nanoparticles doped with Ac-225 and sequestered daughters for targeted alpha therapy. Cancer Biother Radiopharm. 2014; 29:34–41. [PubMed: 24102173]

114. Matson ML, Villa CH, Ananta JS, Law JJ, Scheinberg DA, Wilson LJ. Encapsulation of alpha-particle-emitting $^{225}Ac^{3+}$ ions within carbon nanotubes. J Nucl Med. 2015; 56:897–900. [PubMed: 25931476]

115. Kemp JA, Shim MS, Heo CY, Kwon YJ. “Combo” nanomedicine: co-delivery of multi-modal therapeutics for efficient, targeted, and safe cancer therapy. Adv Drug Deliv Rev. 2016; 98:3–18. [PubMed: 26546465]

116. Radovic M, Vranjes-Duric S, Nikolic N, Jankovic D, Goya GF, Torres TE, et al. Development and evaluation of ^{90}Y-labeled albumin microspheres loaded with magnetite nanoparticles for possible applications in cancer therapy. J Mater Chem. 2012; 22:24017–24025.

117. Radovic M, Calatayud MP, Goya GF, Ibarra MR, Antic B, Spasojevic V, et al. Preparation and in vivo evaluation of multifunctional ^{90}Y-labeled magnetic nanoparticles designed for cancer therapy. J Biomed Mater Res A. 2015; 103:126–134. [PubMed: 24616186]

118. Yinghuai Z, Hosmane NS. Applications and perspectives of boron-enriched nanocomposites in cancer therapy. Future Med Chem. 2013; 5:705–714. [PubMed: 23617432]

119. Jhaveri A, Deshpande P, Torchilin V. Stimuli-sensitive nano-preparations for combination cancer therapy. J Control Release. 2014; 190:352–370. [PubMed: 24818767]

120. Liu Y, Rohrs J, Wang P. Advances and challenges in the use of nanoparticles to optimize PK/PD interactions of combined anti-cancer therapies. Curr Drug Metab. 2014; 15:818–828. [PubMed: 25705903]

Biographies

Weifei Lu

Weifei Lu acquired his PhD degree in Biochemistry from Henan Agriculture University (HAU), China in 2014 and is currently an Associate Professor in HAU. As an active member of Chinese Society of Biochemistry and Molecular Biology, his research interest is focused on the development of gene therapy vectors, study of gene functions, protein engineering, and targeted drug delivery. He is now a visiting professor under the supervision of Dr. Hao Hong for design and synthesis of novel PET tracers based on biodegradable nanomaterials and engineered proteins. He also participates actively in different major research projects funded by NSF China.

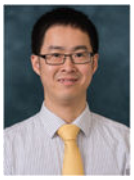

Hao Hong

Hao Hong started his postion as a Research Assistant Professor of Radiology at the University of Michigan in 2014. He received his PhD degree in Biochemistry and Molecular Biology from Nanjing University (P.R. China) in 2008. He acquired his postdoctoral training from 2008 to 2013 in the Department of Radiology, University of Wisconsin, Madison. His research interest is in the design and optimization of new imaging tracers for cancer as well as modification/application of nanomaterials for image-guided therapeutic delivery. Dr. Hong has published >90 peer-reviewed manuscripts (citation >3400 in Google scholar) and received many awards.

Weibo Cai

Weibo Cai is currently an Associate Professor of Radiology and Medical Physics at the University of Wisconsin-Madison. He received his PhD in Chemistry from UC San Diego in 2004. After postdoctoral training at Stanford University, he launched his career at UW-Madison in early 2008. His research is primarily focused on molecular imaging and nanotechnology (http://mi.wisc.edu/), investigating the biomedical applications of various agents developed in his laboratory for imaging and therapy of cancer and cardiovascular diseases. Dr. Cai has authored ~200 peer-reviewed publications with H-index of >50, received many awards, and served on numerous grant review panels.

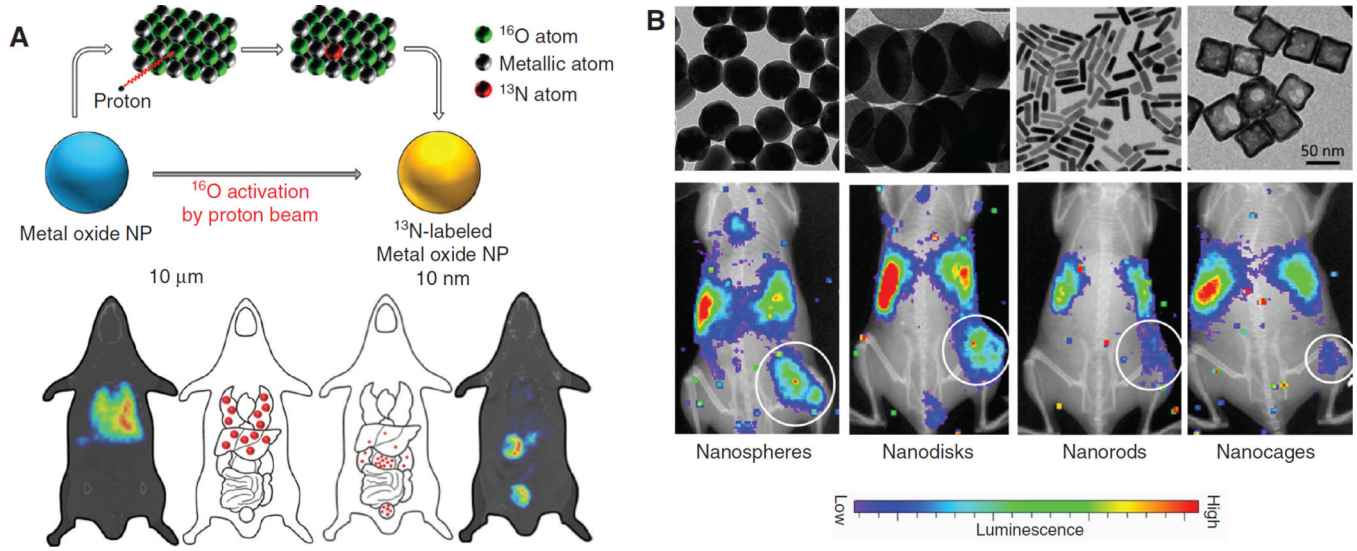

Figure 1.

The utilization of radio-nanomaterials to determine kinetics from parent materials. (A) Formation of ^{13}N-labeled Al_2O_3 nanoparticles. The resulting radio-nanomaterials can help to determine the size-organ distribution relationship. Adapted from reference (14). (B) Use of ^{198}Au-incorporated gold nanomaterials to study the relationship of shape-tumor uptake by Cerenkov imaging. Four nanostructures were studied: nanospheres, nanodisks, nanorods, and cubic nanocages. Adapted from reference (15).

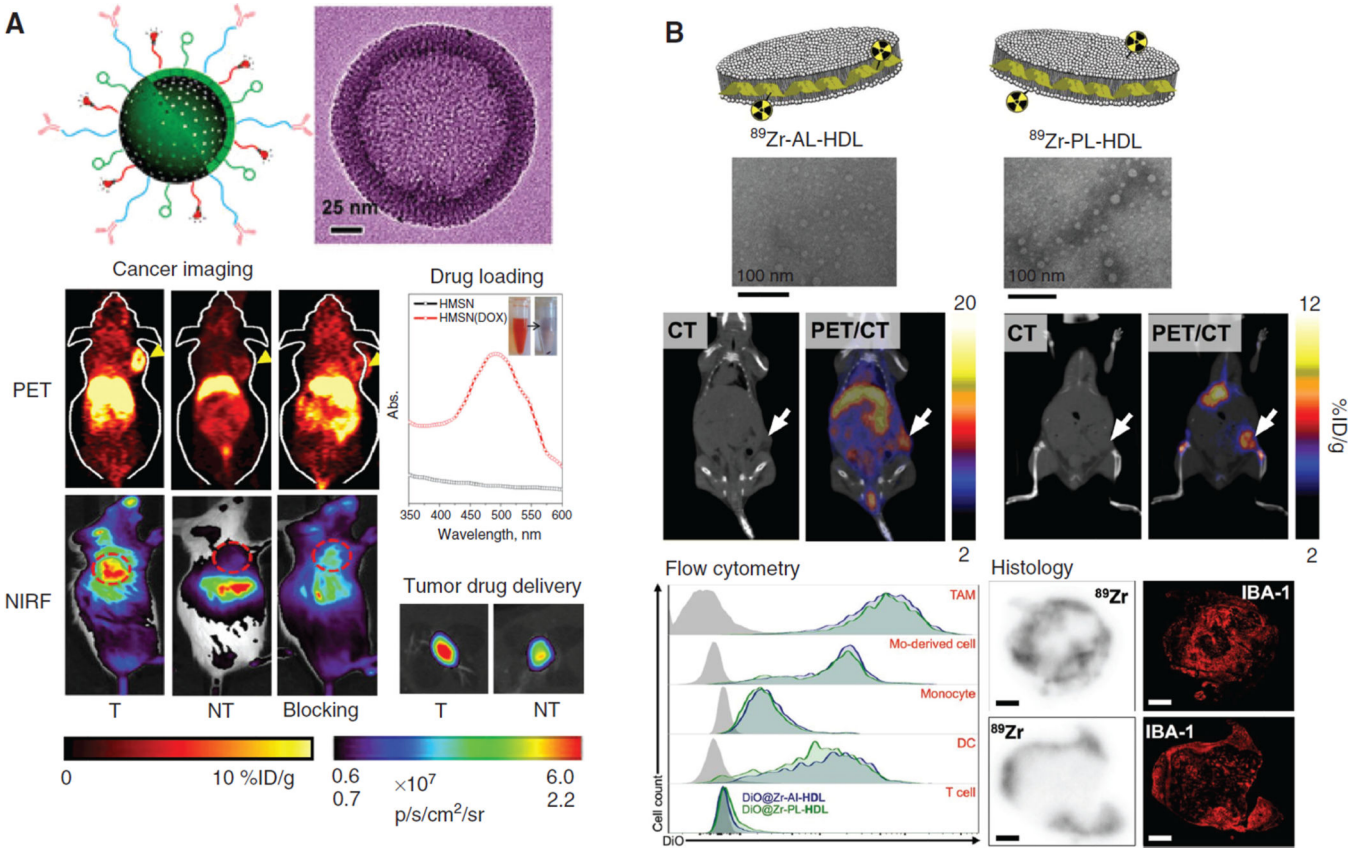

Figure 2.

The utilization of radio-nanomaterials for detection of tumors or tumor-associated cell sub-population. (A) ^{64}Cu-labeled, antibody-conjugated hMSN for targeting of 4T1 tumor in vivo. Both PET imaging and NIRF imaging confirmed the enhanced accumulation hMSN post antibody conjugation. The improved drug delivery efficiency was also confirmed after loading of doxorubicin onto hMSN via fluorescence imaging in tumor. T, Targeted group; NT, non-targeted group. Adapted from from reference (42). (B) ^{89}Zr-labeled HDL nanoparticles for imaging of TAMs. Two types of ^{89}Zr-labeling strategies (on apoA-1 [AL] or on phospholipid [PL]) were adopted. The resulting HDL nanoparticles demonstrated strong accumulation in 4T1 tumors. Both flow cytometry and histology examination showed the preferred uptake of these ^{89}Zr-labeled HDL nanoparticles in TAMs. Adapted from reference (43).

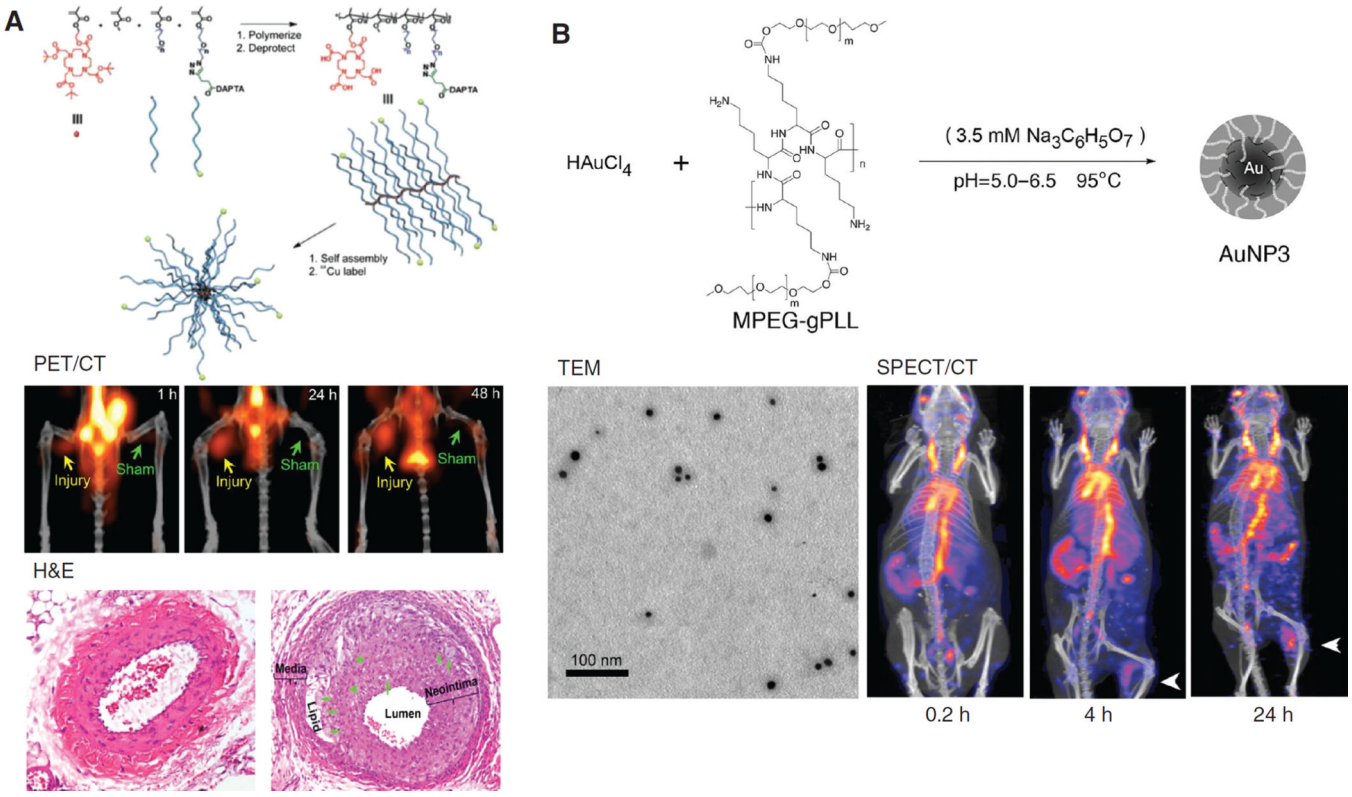

Figure 3.

Imaging of cardiovascular disease and inflammation with radio-nanomaterials. (A) Use of ^{64}Cu-labeled, DAPTA-conjugated comb nanoparticles for imaging of wire-injury induced atherosclerosis. Significantly higher uptake of these nanoparticles was found in the injury area compared with sham-operated area. Histology examination confirmed the progressive atherosclerotic plaque in the injury group. Adapted from reference (57). (B) The structure and morphology of mPEG-gPLL grafted AuNPs and their application in detection of an experimental inflammation via SPECT/CT post ^{99m}Tc labeling. Arrows indicated the location of inflammation. Adapted from reference (58).

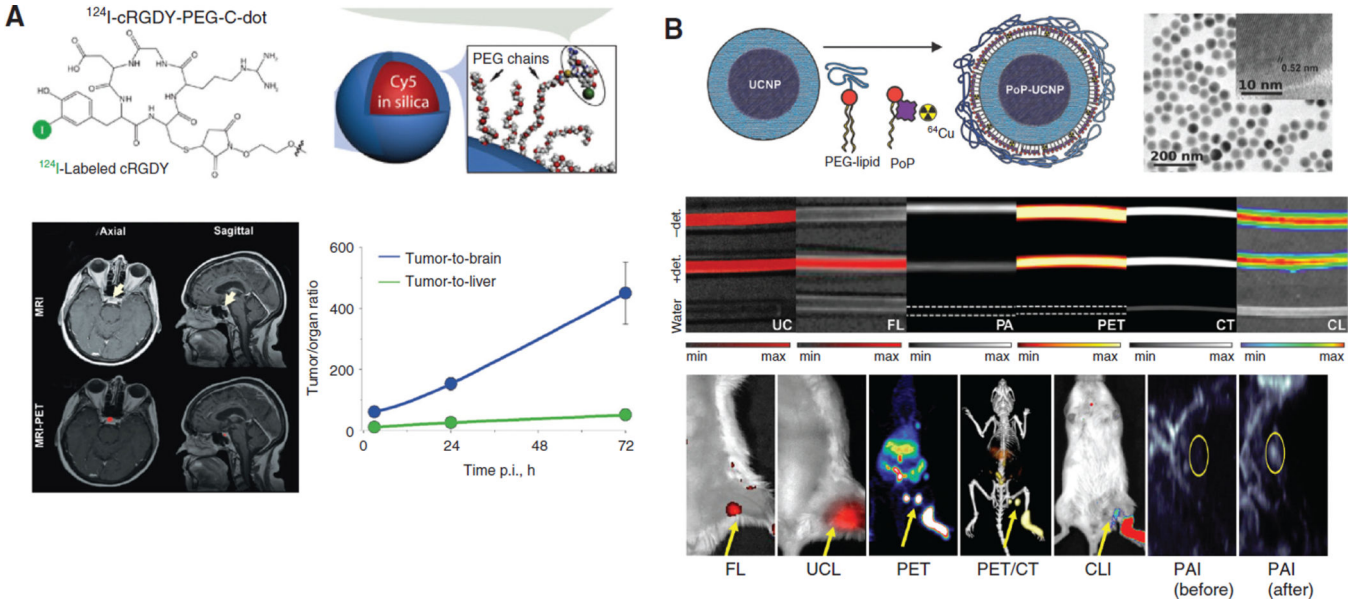

Figure 4.

Radio-nanomaterials for multi-modal imaging. (A) First-in-human clinical trial using ^{124}I-RGD-C-dots(Cy5) for detection of pituitary lesion from metastatic melanoma by PET/MRI. Extremely high tumor-to-background ratios were achieved in these patients. Adapted from reference (83). (B) Hexamodal imaging with a radiolabeled, core-shell structured UCNP-liposome complex. In vitro analysis and in vivo LN mapping were both achieved with these nanocomplex in CT, PET, UCL, Cerekov luminescence, PAI, and fluorescence imaging. Adapted from reference (84).

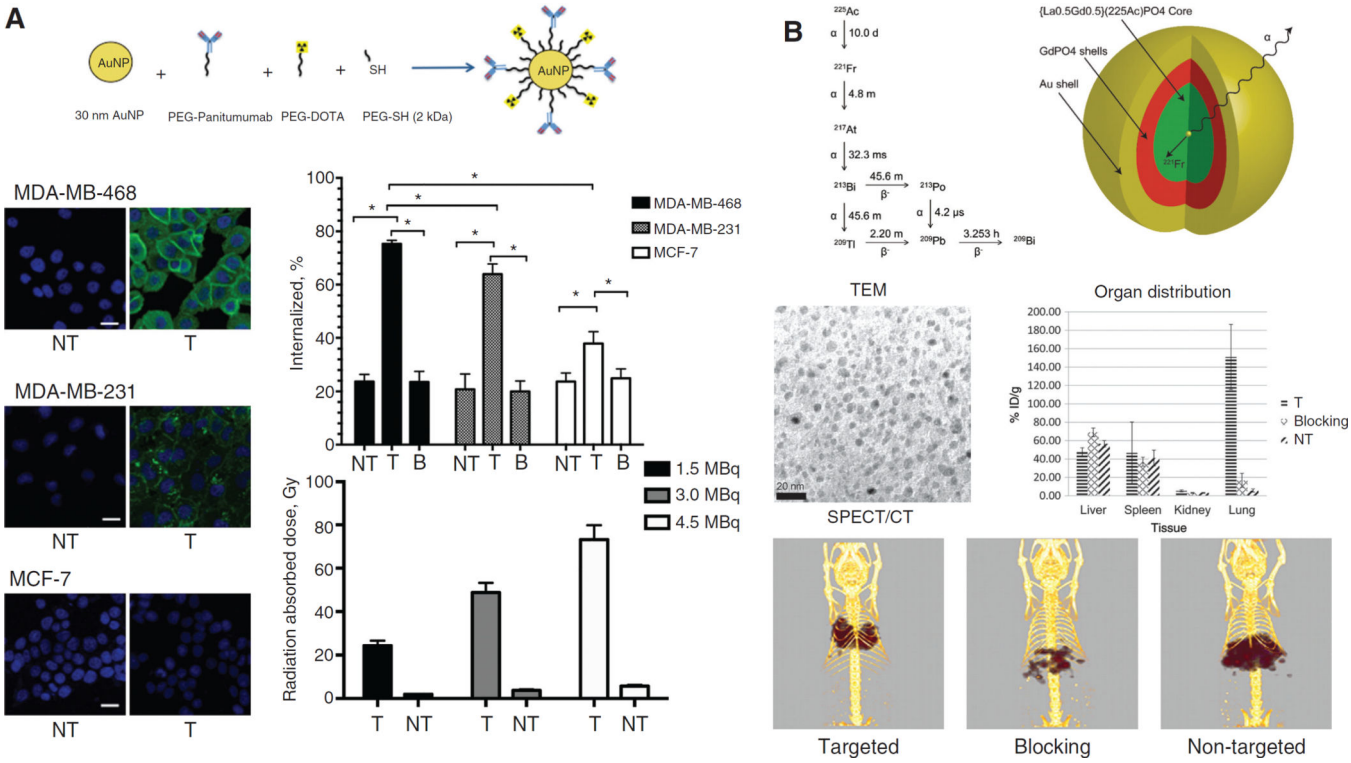

Figure 5.

Therapeutic applications with β-emitter and α-emitter containing radio-nanomaterials. (A) ^{177}Lu-labeled, panitumumab-conjugated AuNPs for radiation delivery into breast cancer cells with different EGFR level. MDA-MB-468: EGFR-high; MDA-MB-231: EGFR-medium; MCF-7: EGFR-low. Both cellular fluorescence images and radioactivity measurement confirmed that conjugation of panitumumab could help AuNPs to deliver high dose of radiation (up to 73.2±6.7 Gy) into the cell nucleus. NT, non-targeted; T, targeted; B, blocking. Adapted from reference (98). (B) Gold-coated GdPO nanoparticles were successfully used to trap ^{225}Ac and its daughter isotopes for targeted alpha therapy. By conjugation of an antibody against thrombomodulin receptors (expressed in lung endothelium), these nanocomplexes demonstrated selective accumulation in the lungs, which was monitored by SPECT/CT. Adapted from reference (99).

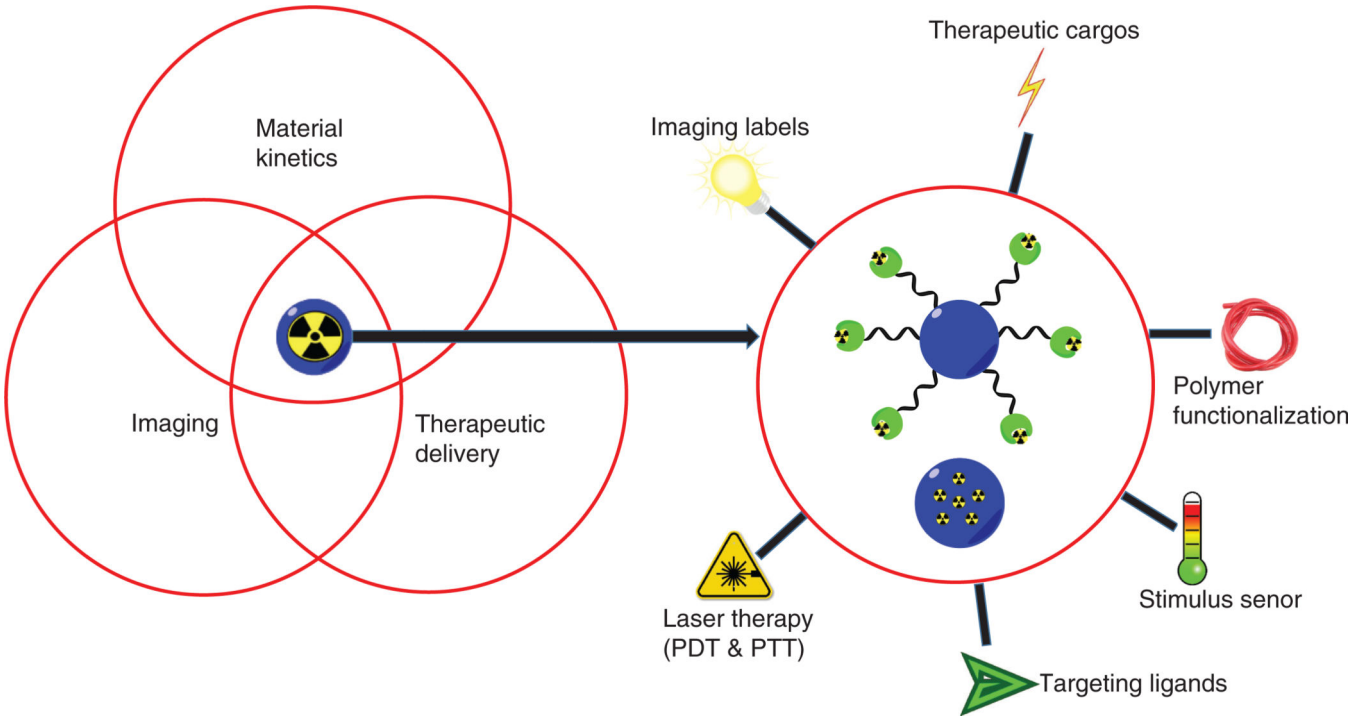

Scheme 1.
Biomedical applications of radio-nanomaterials.

Table 1

Commonly used isotopes for production of radio-nanomaterials.

Isotope	Half-life	Incorporation method into nanomaterials	Production method	Availability	Cost	Utilization
^{18}F	110 min	Post-production labeling; precursor	^{18}O(p, n) ^{18}F	On-site cyclotron	**$$**	Imaging
^{64}Cu	12.7 h	Post-production labeling; precursor; ion exchange	^{64}Zn(n, p)^{64}Cu	Specific cyclotron production needed	**$$**	Imaging; radiotherapy; auger-electron therapy
^{89}Zr	78.4 h	Post-production labeling; precursor	^{89}Y(p, n) ^{89}Zr	Specific cyclotron production needed	**$$$**	Imaging
^{13}N	9.97 min	Proton activation	^{16}0(p, α) ^{13}N	Specific cyclotron production needed	**$$$**	Imaging
^{68}Ga	68 min	Post-production chelation	^{68}Ge/^{68}Ga generator	Generator	**$$**	Imaging
^{59}Fe	44.6 years	Post-production labeling	Neutron activation	Nuclear reactor needed	**$$$**	Material distribution measurement
^{111}In	2.8 days	Chelation	^{111}Cd(p, n)^{111}ln	Commercially available	**$$**	Imaging; radiotherapy
^{99m}TC	6h	Chelation	^{99}Mo/^{99m}Tc generator	Generator	**$**	Imaging
^{177}Lu	6.7 days	Chelation	^{176}Yb(n,γ)^{177}Yb→^{177}Lu	Commercially available	**$$$**	β-therapy
90γ	64.1 h	Chelation	^{90}Sr/^{90}Y generator	Generator	**$$**	β-therapy
^{225}Ac	10 days	Embedded inside the nanomaterials	^{226}Ra (γ, n) ^{225}Ac	Specific cyclotron production needed	**$$$**	α-therapy

Eur J Nanomed. Author manuscript; available in PMC 2017 July 01.

Table 2

Representative radio-nanomaterials for biomedical applications.

Radio-material	Labels	Material characteristics	Major application(s)	Research stage	Production cost
Silica-based nanomaterials	^{124}I ^{64}Cu ^{89}Zr	Biocompatibility, biodegradability, superior cargo-loading capacity	Cancer imaging, therapeutic delivery	Clinical test (Cornell dots); small-animal test	**$**
Carbon nanomaterials	^{64}Cu, ^{124}I, ^{111}In, ^{66}Ga, ^{225}Ac, etc	Photothermal effect, Gd-loading (fullerene)	Cancer imaging, stimulus-responsive therapeutic delivery, radiotherapy	Mostly in small animals. SWNTs were tested for ^{225}Ac loading. Clinical test can be foreseen	$$ (fullerene can be $$$)
IONPs	^{64}Cu, ^{69}Ge, ^{111}In, ^{14}C, ^{72}As, etc	Paramagnetic properties, biocompatibilitytd	Disease imaging	Mostly in small animals. Radiolabeled IONPs have not been tested in human	**$$**
Gold nanomaterials	^{68}Ga, ^{64}Cu, ^{198}Au, ^{177}Lu, etc	Optical emissions (e.g. for CRET), biocompatibility	Disease imaging, radiotherapy	Mostly in small animals	**$$**
QDs	^{64}Cu, ^{18}F, etc	Optical emissions	Cancer imaging	Mostly in small animals	**$$**
UCNPs	^{18}F, ^{153}Sm, etc	UCL emissions, magnetic properties (with doping)	Cancer imaging	Cell or rodents-based studies	**$$$**
Metal oxide nanomaterials (other than IONPs)	^{64}Cu, ^{99m}Tc, ^{225}Ac, etc	Stable cargo-loading, unique physical properties	Cancer imaging, radiotherapy	Cell or rodents-based studies	**$ — $$$**
Polymer-based nanomaterials	^{99m}Tc, ^{89}Zr, ^{64}Cu, ^{188}Re, ^{90}Y, etc	Biocompatible, chemically versatile	Cancer/inflammation imaging, radiotherapy	Cell or rodents-based studies	**$$**
Lipid-containing nanomaterials	^{89}Zr, ^{64}Cu, etc	Biocompatible, chemically versatile	Cancer/inflammation imaging, therapeutic delivery	Cell or rodents-based studies	**$**